THE UNIVERSITY OF CHICAGO

UNDERSTANDING AND OVERCOMING THE NON-T CELL-INFLAMED TUMOR MICROENVIRONMENT

A DISSERTATION SUBMITTED TO

THE FACULTY OF THE DIVISION OF THE BIOLOGICAL SCIENCES

AND THE PRITZKER SCHOOL OF MEDICINE

IN CANDIDACY FOR THE DEGREE OF

DOCTOR OF PHILOSOPHY

COMMITTEE ON IMMUNOLOGY

BY

EMILY FAYE HIGGS

CHICAGO, ILLINOIS

DECEMBER 2021

TABLE OF CONTENTS

List of Figures v
List of Tables vi
Acknowledgements vii
Abstract x
Chapter 1: Introduction 1
1.01 Tumors evade immune destruction 1
1.02 Innate immune recognition of cancer 2
1.03 STING agonists as a cancer therapeutic 4
1.04 Rational combinations of innate immune agonists 6
1.05 The non-T cell-inflamed tumor microenvironment 8
1.06 Mechanisms of tumor immune exclusion 11
1.07 Wilms tumor as a severely non-T cell-inflamed cancer type 14
Chapter 2: Materials and Methods 16
2.01 Cell lines and culture conditions 16
2.02 In vitro stimulation assays 16
2.03 Quantitative real-time PCR 17
2.04 Immunofluorescent imaging Flow Cytometry 17
2.05 NF-κB reporter assay 18
2.06 Ex vivo stimulation 18
2.07 Transplantable tumor model 20
2.08 Genetically engineered mouse (GEM) tumor model 20
2.09 In vivo agonist and antibody treatment 20
2.10 Tissue processing and immune cell isolation 22
2.11 Flow cytometry of tumor-infiltrating immune cells 22
2.12 Immunofluorescence of human tissue samples 23
2.13 Multispectral scanning and image analysis 24
2.14 Analysis of RNA sequencing data 25
2.15 Statistical analysis 25
Chapter 3: TLR4 agonist LPS augments STING-induced innate immune activation 27
3.01 Introduction 27
3.02 LPS synergizes with DMXAA in vitro 27
3.03 LPS does not augment DMXAA signaling through STING or IRF3 activation 29
3.04 LPS signaling through NFκB is required for synergy 30
3.05 LPS synergizes with DMXAA in vivo to promote tumor control 32
3.06 Summary of Findings 34
Chapter 4: Flt3L promotes CD103$^+$ DC accumulation in non-T cell-inflamed β-catenin-expresing tumors 36
4.01 Introduction 36
4.02 DMXAA increases CD8$^+$ T cell but not CD103$^+$ DC infiltration in BPC tumors 36
4.03 DMXAA does not sensitize BPC tumors to αPD-L1 + αCTLA-4 immunotherapy 39
4.04 Flt3L induces CD103$^+$ DC infiltration in BPC tumors 41
4.05 Flt3L + DMXAA does not significantly improve tumor control in BPC mice 42

4.06 Flt3L + DMXAA significantly improves tumor control in BPC mice treated with αPD-L1 + αCTLA-4 44
4.07 Summary of Findings 45
Chapter 5: Low tumor immunogenicity is associated with high DNA repair gene expression 47
5.01 Introduction 47
5.02 Wilms tumor samples demonstrate low T cell inflammation scores 47
5.03 DNA damage response genes are upregulated in Wilms tumors 49
5.04 DNA repair gene expression negatively correlates with T cell inflammation in adult cancers 53
5.05 DNA repair gene expression associates with T cell inflammation independent of mutation burden 55
5.06 $MSH2^+$ tumor cells negatively correlate with $CD8^+$ T cells in melanoma and are associated with immunotherapy response 56
5.07 Summary of findings 59
Chapter 6: Discussion 61
6.01 STING agonist promise and limitations as a cancer therapeutic 61
6.02 Synergy between innate pathways improves IFN-β production and tumor control 64
6.03 Flt3L can overcome the $CD103^+$ DC defect in BPC tumors 66
6.04 DNA damage triggers innate immune activation 67
6.05 Overexpression of DNA repair genes may limit immune activation 68
6.06 Conclusions 69
References 72

LIST OF FIGURES

Figure 3.1 LPS and STING agonist DMXAA synergize to induce IFN-β transcription. 28
Figure 3.2 LPS does not strongly affect STING aggregation or IRF3 nuclear translocation. 30
Figure 3.3 LPS promotes NFkB activation by increasing p65 nuclear translocation. 32
Figure 3.4 Intratumoral LPS improves tumor control alone and in combination with DMXAA. 33
Figure 3.5 In vivo benefit of DMXAA and LPS combination is dependent on STING and TLR4. 34
Figure 3.6 Working model of synergy between LPS and DMXAA. 35
Figure 4.1 DMXAA dose response in BPC tumors 37
Figure 4.2 DMXAA significantly increases $CD8^+$ T cell numbers but not $CD103^+$ DC numbers38
Figure 4.3 DMXAA does not improve BPC tumor control or sensitize to anti-PD-L1 + anti-CTLA-4 40
Figure 4.4 Flt3L dose response in BPC tumors 42
Figure 4.5 Flt3L does not improve BPC tumor control or sensitize to DMXAA therapy 43
Figure 4.6 Flt3L and DMXAA sensitize tumors to anti-PD-L1 + anti-CTLA-4 45
Figure 5.1 Wilms tumors have lower TIS than other pediatric cancer types, adult kidney cancer types, and matched normal kidney samples. 49
Figure 5.2 Genes upregulated in Wilms tumor and anti-correlated with TIS associate with DNA damage response and repair pathways. 50
Figure 5.3 Method for developing DNA repair score. 52
Figure 5.4 Wilms tumors have higher DNA repair scores than other pediatric cancer types, adult kidney cancer types, and matched normal kidney samples. 53
Figure 5.5 TIS significantly anti-correlates with DNA repair score in most TCGA tumor types, including melanoma. 54
Figure 5.6 TIS does not strongly associate with total mutation count in melanoma and DNA repair score correlation with TIS is not explained by mutation count, Type I IFN score, or proliferation score. 56
Figure 5.7 MSH2 expression significantly anticorrelates with TIS in most TCGA tumor types, including melanoma. 57
Figure 5.8 MSH2+ tumor cell numbers significantly anti-correlate with CD8+ T cells in melanoma patients and are significantly higher in non-responders to checkpoint blockade immunotherapy. 59

LIST OF TABLES

Table 2.1. Mouse qRT-PCR primers 17
Table 2.2 Immunofluorescent imaging antibodies..... 18
Table 2.3 Flow cytometry antibodies to assess CD11c purity..... 19
Table 2.4 Flow cytometry antibodies to assess $CD8^+$ T cell depletion 21
Table 2.5 Flow cytometry antibodies to assess tumor immune infiltrates..... 23
Table 5.1 DNA repair genes upregulated in Wilms tumors span multiple pathways. 51

ACKNOWLEDGEMENTS

The thesis presented here is the result of a truly collaborative effort and I am deeply grateful to those who contributed to my scientific and personal development during these PhD years.

First and foremost, I would like to thank my thesis advisor, Dr. Thomas Gajewski, for his unyielding support, encouragement, and guidance. Your enthusiasm for science is infectious, and I distinctly remember leaving each meeting in your office excited to plan experiments and test the new ideas we discussed. You taught me the value in composing scientific data as a story and I am consistently impressed by your ability to craft a compelling argument. I have so much respect for your approach to science and your relentless drive to tackle important, interesting questions. My time in the Gajewski laboratory was an absolute privilege, and I feel fortunate to have been given the opportunity to learn from one of the greats.

Several other members of the laboratory were instrumental in my development and made the experience a joy as well. Blake Flood trained me when I joined and taught me so much about immunology and experimental techniques that I will always appreciate. I'd also like to thank the other core graduate students I worked alongside: Jessica Fessler, Kyle Cron, and Alexandra Cabanov. I always found our scientific discussions enriching and consider you all to be close friends. The laboratory environment would not have been complete without the amazing postdoctoral scholars Andrea Ziblat, Shuyin Li, and Vyara Matson and fellows Jonathan Trujillo, Athalia Pyzer, and Sherin Rouhani. I'm so grateful to have been able to collaborate with you and learn about the next phases of the career path through your mentorship. My PhD training also benefited greatly from my interactions with former lab members Jason Williams, Stefani Spranger, and Brendan Horton. Thank you for your guidance and expertise. Lastly, to the newer members of the Gajewski laboratory: Santiago Acero Bedoya, Valeria Rios, and Anna Martinez, it was an absolute pleasure working with you and I can't wait to see the great things you go on to accomplish.

Prior to joining the Gajewski laboratory, I had two incredible research mentors, Dr. Michael Glotzer and Dr. Murray Korc. My experience in your laboratories confirmed my passion for biological science and helped hone my research interests. The opportunity for me to pursue a PhD would not have been possible without the Growth, Development, and Disabilities Training Program (GDDTP). Nancy Schwartz and Laurie Risner administer the program and have been incredibly supportive throughout my journey. I am grateful to have been funded by the GDDTP T32 training grant as well as an individual National Cancer Institute F30 training grant and a Melanoma Research Foundation Medical Student Grant Award.

I would like to thank my thesis committee members Anita Chong, Nicolas Chevrier, and Aly Khan for their insights and suggestions on my thesis work. Your diverse research perspectives allowed me to see my projects in a new light, and I wish I had time to test all the ideas you put forward in my committee meetings. Other faculty at the University of Chicago have been instrumental in my immunology training, and faculty participation in immunology program events created a vibrant intellectual culture from which I benefited greatly. I would particularly like to thank Marisa Alegre and Albert Bendelac for their thoughtful inputs on my thesis.

My work would also not have been possible without several core facilities at the University of Chicago. I would first like to thank the Animal Resources Center and the many mice that went into this research. Karin Kelly and Giovanna Cristopher as well as the other veterinarians and technicians have all been incredible. I am so appreciative for all that you do to ensure the humane and ethical care of the animals we use for research. I would also like to thank the teams at the Cytometry and Antibody Technology Core Facility and the Genomics Core Facility. So much important research depends on these cores running smoothly and I thank you for all your efforts and troubleshooting to ensure the highest possible quality data get generated. Thank you to Riyue Bao from the Center for Research Informatics; you taught me so much about bioinformatics techniques and I really appreciate your mentorship.

My graduate school experience would not have been the same without the other students in the Committee on Immunology, especially Martin Sepulveda, Jen Allocco, and Jordan Voisine. Thank you for being great study partners and friends and for enriching this experience overall. I found so much joy through activities in Chicago and would specifically like to thank the Major Taylor Cycling Club and Jackson Park Yacht Club for incorporating me into your communities. Lastly, I could not have finished this PhD without the loving support from my parents and siblings -- it means more to me than you will ever know.

ABSTRACT

Checkpoint blockade immunotherapies have demonstrated remarkable therapeutic success by overcoming tumor-induced T cell inhibition, however their efficacy is poor when patients lack evidence of a spontaneous T cell response. Tumors in mice which generate a spontaneous T cell response activate the innate immune system through the STING pathway. STING agonists promote dendritic cell (DC) activation as well as subsequent priming and recruitment of T cells, leading to significant tumor control in transplantable models. However, preliminary clinical trial results suggest that STING agonists have clinical activity in only a minority of patients and have limited efficacy in non-inflamed tumors. This observation suggests a need to more closely study the non-inflamed tumor microenvironment and understand which innate immune cells and signaling pathways are required for driving tumor-specific T cell priming and recruitment in this context. Given that pathogen encounter rarely activates a single innate immune pathway, we began by investigating different TLR pathways for their potential to augment innate immune activation induced by STING. We found that the TLR4 agonist LPS was able to synergize with the STING agonist DMXAA to induce IFN-β production *in vitro* and was able to improve tumor control *in vivo*. We next addressed the possibility that STING agonists could fail due to insufficient numbers of essential DCs present in the tumor microenvironment. We found that intratumoral Flt3L promoted accumulation of $CD103^+$ DCs and led to tumor control in combination with DMXAA and anti-PD-L1 + anti-CTLA-4 in our non-T cell-inflamed genetic mouse melanoma model. Lastly, we investigated gene expression profiles of Wilms tumors, a severely non-T cell-inflamed cancer type. We identified upregulation of DNA repair gene expression in these tumors as well as various adult tumor types including melanoma, suggesting a previously undescribed mechanism of immune evasion.

Chapter 1: Introduction

1.01 Tumors evade immune destruction

The human immune system is highly evolved to rid the body of a wide range of pathogens and infected cells. Cancers can arise when somatic cells acquire mutations that convey a growth or survival advantage. These neoplastic cells are often recognized and destroyed by the immune system, but in cases in which this does not occur completely, selective pressure from immune surveillance can lead to outgrowth of the most resilient cell subsets[1,2]. As these cells grow into a new tissue, they can exploit endogenous tissue repair and wound healing mechanisms. This process may attract additional immune attention, driving a complex and dynamic interaction between the nascent tumor and the immune system[3]. The way in which the immunological environment shapes the tumor as it develops has been termed cancer immunoediting, and it can favor the outgrowth of tumors adept at evading immune elimination[4,5].

Tumor antigen-specific $CD8^+$ T cells are a critical component of the anti-tumor immune response. Many patients display evidence of an endogenous, de novo T cell response against their tumors, as indicated by transcriptional profiling and presence of activated T cells within the tumor microenvironment. However, those T cells fail to eliminate tumors unaided. The failure of spontaneous immune-mediated tumor rejection is thought, in part, to be due to the action of negative regulatory mechanisms that inhibit key functional properties of T cells infiltrating tumors. One of these pathways involves engagement of the T cell inhibitory receptor, PD-1, by its major ligand, PD-L1[6]. Based on this biology, antibodies targeting the PD-1/PD-L1 interaction have been developed for clinical use and show remarkable activity in a wide range of

tumor types[7]. Clinical activity has been correlated with the presence of an activated T cell gene signature at baseline[8], and following treatment with anti-PD-1, a marked expansion of tumor-infiltrating $CD8^+$ T cells has been observed[9].

Despite these clinical successes, a major subset of cancer patients lacks a spontaneously developed T cell-inflamed tumor microenvironment in the steady state, and generally does not respond to checkpoint blockade immunotherapy[10]. It is thought that triggering productive T cell-based inflammation within the tumor microenvironment may offer the potential to expand the fraction of patients benefiting from anti-PD-1 treatment and other immunotherapies. One strategy towards this goal has been to gain an understanding of the fundamental mechanistic steps involved with spontaneous T cell activation and infiltration against tumors when it does occur, with the aim of mimicking or reproducing those steps in the cases when it does not occur de novo.

1.02 Innate immune recognition of cancer

In general, the generation of an adaptive immune response (i.e., induction of a T cell or antibody response) first requires activation of the innate immune system, which signals the presence of "danger" or an outside threat. In the tumor context, dead and dying cancer cells release antigens that can be taken up, processed, and displayed by antigen presenting cells (APCs). Studies in $Batf3^{-/-}$ mice have implicated Batf3-lineage $CD103^+$ dendritic cells (DCs) as a particularly important APC subset for this process. $CD103^+$ DCs cross-present tumor-derived antigen on major histocompatibility complex (MHC) class I to $CD8^+$ T cells primarily in the tumor-draining lymph node, although some evidence suggests T cell priming may also occur within the tumor microenvironment. Following priming and activation in the lymph node, T cells

traffic back to the tumor where they can carry out their effector function and kill tumor cells. This trafficking is supported by the chemokines CXCL9 and CXCL10 which bind CXCR3 on T cells[11,12]. During the effector phase of the antitumor immune response APCs continue to provide additional activating signals, such as the costimulatory ligands CD80 and CD86, which are capable of promoting T cell expansion, survival, and function within the tumor.

Preclinical models revealed that endogenous $CD8^+$ T cell priming against tumors was markedly reduced in mice deficient for STING (STimulator of INterferon Genes)[13]. STING knockout host mice also showed reduced cytokine production (including IFN-β) in response to tumor implantation and failed to reject highly immunogenic tumors. These defects were not observed in mice deficient in other innate immune pathways, such as specific Toll-like receptors (TLRs). The STING pathway is a cytosolic DNA sensing pathway, and evidence indicated that tumor-derived DNA could be found within the cytosol of tumor-infiltrating APCs. Cytosolic DNA is detected within cells when it binds to the enzyme cyclic GMP-AMP synthase (cGAS), which then generates cyclic GMP-AMP (cGAMP) that acts as a secondary messenger to activate STING and promote downstream signaling[14]. Following cGAMP binding, STING migrates from the ER through the Golgi where TBK1 binds and phosphorylates STING[15]. This complex then buds off in perinuclear vesicles. The transcription factor IRF3 can bind the activated complex and be phosphorylated by TBK1[16]. Phosphorylated IRF3 then translocates to the nucleus where it induces the expression of IFN-β and other genes[17]. In this way, tumor-derived DNA is sensed by cGAS and leads to IFN-β transcription downstream of STING pathway activation.

IFN-β production in the tumor microenvironment is associated with increased expression of the costimulatory molecule CD86 on dendritic cells and increased cross-priming of $CD8^+$ T cells[18]. Chemokine production by activated dendritic cells in the tumor microenvironment is also

critical for recruiting effector T cells[19]. Tumors that lack $CD103^+$ DCs fail to produce CXCL9/10 and activated, tumor-specific T cells cannot efficiently be recruited to the tumor[20]. Mice that lack the type I interferon receptor IFNAR in $CD11c^+$ cells have poor tumor control, presumably due to a failure of dendritic cells to mature and prime T cells as well as produce the chemokines necessary to recruit T cells. In humans, type I interferons are also associated with T cell inflammation in tumors. Previous work in metastatic melanoma demonstrated a positive correlation between activated T cell gene expression and a type I interferon-induced gene expression signature[21].

Together, these observations suggest that STING pathway signaling in the tumor microenvironment promotes IFN-β production, which leads to activation of APCs including $CD103^+$ DCs. Once activated, DCs play a role not only in priming T cells in the tumor-draining lymph node, but also in recruiting them back to the tumor and promoting their expansion and effector function. These data led to the hypothesis that exogenous agonists of the STING pathway may have the potential to trigger de novo innate immune activation, leading to an adaptive immune response that can then control tumor growth.

1.03 STING agonists as a cancer therapeutic

Based on these observations regarding the mechanisms involved in the emergence of endogenous immune responses, intratumoral injection of exogenous STING agonists has been explored as a therapeutic strategy. In multiple transplantable tumor models, intratumoral injection of STING agonists led to rapid rejection of murine tumors[22]. Maximal tumor control depended on $CD8^+$ T cells, confirming an immune component of this efficacy, although some

tumor control was observed in the absence of T cells. STING pathway activation was associated with increased IFN-β expression by tumor-infiltrating immune cells, increased expression of the T cell costimulatory molecule CD86 on APCs, and increased tumor antigen-specific $CD8^+$ T cell cross-priming. These results indicate that providing additional STING pathway activation through pharmacologic manipulation can lead to augmented type I IFN signaling, APC maturation, $CD8^+$ T cell cross-priming, and recruitment of T cells into the tumor microenvironment where they mediate rejection of tumors.

The STING agonist DMXAA was originally characterized as an anti-vascular agent and displayed anti-tumor efficacy in a variety of mouse tumor models in vivo[23,24]. While it fails to bind human STING effectively, in vivo delivery of DMXAA in mice was found to induce a potent adaptive immune response against transplantable tumors, as evidenced by immunologic memory to re-challenge, rejection of distant non-treated tumors, and clearance of metastases. This host response depended on type I IFN signaling and $CD8^+$ T cells, arguing that an adaptive immune response was a major mechanistic component for efficacy[22,25,26]. The failure of DMXAA efficacy in $STING^{-/-}$ mice, as well as lack of activation of $STING^{-/-}$ APCs in vitro, together argued that DMXAA was indeed a direct STING agonist and that activity depended on host expressed STING.

Based on lack of DMXAA binding to human STING, it became desirable to identify new chemical entities with the potential to activate human STING for immune activation in the setting of cancer. Initial drug development focused on using cyclic dinucleotides as a starting point to mimic natural STING agonists but with increased stability and activation of the five major human STING allelic variants. The first generation of human STING agonists, including MIW815 (ADU-S100) and MK-1454, have been investigated in early phase clinical trials alone

and in combination with anti-PD-1. So far, some clinical responses to these agonists have been observed, but only in a minority of patients[27,28]. Multiple next generation STING agonists or inhibitors of STING regulatory proteins are being advanced into clinical development though clinical data have not yet been reported. These include approaches that attempt to improve the potency of the molecule while limiting the deleterious impact of STING agonists on activated T cells at high doses, to limit non-canonical NK-κB activation (which lead to elaboration of IL-6 and TNF-α), as well as to facilitate systemic administration approaches that do not require intratumoral injection.

Several biological considerations are being explored to understand mechanisms of STING agonist response versus resistance. These include deciphering which immune cells in the tumor microenvironment must be present for STING agonists to induce downstream immune priming, understanding the optimal dose and schedule of STING agonists to avoid overstimulation and negative regulation, and identifying predictive biomarkers for clinical activity.

1.04 Rational combinations of innate immune agonists

The results from early clinical data showing STING agonists alone result in tumor shrinkage in only a subset of patients indicate that deeper knowledge of innate immune pathway activation in response to cancer is needed. In the case of pathogen exposure, innate immune sensing rarely occurs by activating only one signaling pathway, and mammalian organisms have evolved multiple discreet innate immune sensing receptor systems leading to the downstream activation of several transcription factors. The detection of pathogen associated molecular

patterns (PAMPs) or danger associated molecular patterns (DAMPs) from damaged tissue by specific receptors allows the innate immune system to distinguish between threats and tailor downstream responses accordingly.

A major class of innate receptors for detecting pathogens are the Toll-like receptors (TLRs). TLRs are pattern recognition receptors that reside on the cell surface or in endosomes of various immune cells. They recognize microbial protein or lipid components as well as single or double stranded RNA or unmethylated CpG DNA[29]. TLR signaling leads to activation of transcription factors such as NFκB, IRF3, and IRF7, and contributes to the production of proinflammatory cytokines including type I IFNs, TNFα, IL-6, and IL-1β[30]. In addition to cytokine production, TLR activation promotes costimulatory molecule expression on macrophages and DCs, providing an important link between innate and adaptive immune responses.

The IFN-β enhancer contains binding sites for multiple transcription factors, including IRF3, IRF7, NFκB, and AP1, and it is likely that a combination of multiple signaling pathways and downstream transcription factors is necessary for optimal IFN-β transcription[31,32]. In fact, it has been reported that maximal IFN-β transcription is only achieved when all four transcription factor binding sites are present and cells are stimulated with a complex challenge, such as a virus. Stimulation with agonists known to activate these transcription factors individually were unable to elicit strong IFN-β production.

Because the activation of multiple transcription factors can contribute to IFN-β transcription, the IFN-β enhancer is a potential point of interaction between multiple innate immune signaling pathways to impact on IFN-β transcription. This notion led to the idea that a

deeper understanding of STING pathway interaction with TLR pathways could inform novel approaches to augment IFN-β production in in the context of cancer.

Activating TLR pathways as a strategy to combat cancer is not a novel concept. In fact, William B. Coley, often considered the "Father of Immunotherapy," first injected streptococcal organisms into a patient with inoperable cancer in 1891[33,34]. He went on to treat over 1000 patients with bacteria or bacterial products, and reported remarkable tumor responses, especially in bone and soft tissue sarcomas[35]. Despite its clinical promise, 'Coley's toxin' was not well received by the scientific community and it was not until decades later that Coley's work regained recognition. Currently there are several TLR agonists in clinical development, and the TLR7 agonist Imiquimod has been FDA approved in basal cell carcinoma among other indications[36]. Additional preclinical and clinical data suggest that achieving successful antitumor responses in a large fraction of patients requires combinatorial approaches[37]. Pursuing rational combinations of STING agonists and TLR agonists has the potential to limit deleterious effects of high dose STING agonist administration and potentially increase the fraction of patients who respond to STING agonist therapy.

1.05 The non-T cell-inflamed tumor microenvironment

Another reason therapeutic STING agonists may be unsuccessful in generating productive T cell responses in patients is that some tumors lack the required $CD103^+$ DC subset for T cell priming and recruitment. This notion suggests a need to more closely study the non-inflamed tumor microenvironment and understand which innate immune cells and signaling pathways are required for driving tumor-specific T cell priming and recruitment in this context.

One useful tool to address these questions is the BRAF-activated, PTEN-deleted, β-catenin-stabilized (BPC) genetic melanoma model.

Unlike BRAF-activated, PTEN-deleted (BP) tumors, BPC tumors have an additional stabilizing β-catenin mutation, which mechanistically has been shown to lead to poor infiltration of both $CD103^+$ dendritic cells and $CD8^+$ T cells. This phenotype was associated with lack of therapeutic activity of checkpoint blockade immunotherapy[38]. Presumably due to the low number of $CD103^+$ DCs, there was a deficit in T cell priming, with significantly reduced SIY-specific T cell numbers when BPC tumors also inducible expressed the model antigen SIY (BPC-SIY). In addition to poor T cell priming, a separate, additional defect was identified in the recruitment of primed effector tumor-specific T cells into tumor sites. Pre-activated, SIY-specific 2C T cells when transferred into BPC-SIY animals did not accumulate in the tumor and failed to exert therapeutic activity[38].

As mentioned above, BP tumors were infiltrated by Batf3-lineage $CD103^+$ DCs, which are the subset particularly important for cross-priming tumor-specific T cells and recruiting activated T cells into the tumor. When BP host mice were engrafted with $Batf3^{-/-}$ bone marrow they no longer displayed spontaneous T cell accumulation. Microarray data showed that BPC tumors have significantly lower expression of chemokines, such as CCL4 and CCL5, which are known to bind CCR5 and promote $CD103^+$ DC recruitment. In BP tumors, $CD103^+$ but not $CD103^-$ DCs expressed high levels of CCR5, and BP host mice engrafted with $CCR5^{-/-}$ bone marrow showed a significant reduction in tumor-infiltrating $CD103^+$ DCs. CCR5 is a chemokine receptor known to be important for regulating DC migration to inflamed tissues[39]. BP host mice lacking CCR5 in the hematopoietic compartment also demonstrate significantly reduced T cell

infiltration, suggesting that CD103$^+$ DCs are additionally necessary for effector T cell recruitment[20].

In BP mice crossed to STING$^{-/-}$ mice there was a loss of T cell recruitment but not CD103$^+$ DC recruitment. This observation indicates that DCs unable to respond to endogenous STING agonists fail to prime and recruit T cells to the tumor, which supports the previously described results observed in transplantable tumor models. In BP tumors, tumor-infiltrating APCs also produced IFN-β, and CD103$^+$ DCs were the predominant source of CXCL9 and CXCL10. BP-SIY mice reconstituted with CXCL10$^{-/-}$ bone marrow were unable to recruit transferred effector 2C T cells, and when DCs were depleted using a CD11c-DTR bone marrow chimera, Flt3 ligand-bone marrow-derived wild type but not CXCL10$^{-/-}$ DCs were able to recover 2C T cell accumulation. These results prove the requirement for CXCL10 production by dendritic cells for tumor-specific T cell recruitment to BP tumors[20].

While BPC tumors lacked spontaneous infiltration of CD103$^+$ DCs and subsequent priming and recruitment of CD8$^+$ T cells, intratumoral injection of in vitro-activated, Flt3 ligand-bone marrow-derived DCs (BMDCs) was shown to reverse those defects at least partially. Injected tumors were able to accumulate transferred effector 2C T cells, as well as to significantly delay tumor growth and sensitize BPC tumors to checkpoint blockade antibodies[38]. This observation serves as a proof-of-principle that non-inflamed tumors can prime and recruit tumor-specific CD8$^+$ T cells to generate a productive immune response if the appropriate activated DCs are present.

Thus, the BPC melanoma model presents an enticing opportunity to evaluate strategies aimed at recruiting DCs, specifically the CD103$^+$ DC subset, to non-inflamed tumors. If this can be achieved successfully, it may sensitize these tumors to STING agonist and/or checkpoint

blockade antibody therapy. If translatable to the clinic, such strategies would have the potential to expand the fraction of patients who receive clinical benefit from these existing immunotherapies. By continuing to refine our understanding of the necessary steps involved in generating a successful anti-tumor immune response, we may be able to identify and overcome defects further upstream in the process and maximize clinical responses.

1.06 Mechanisms of tumor immune exclusion

The current success of immunotherapy is limited by the prevalence of non-T cell-inflamed tumors which typically do not respond to checkpoint blockade antibodies[40]. This necessitates study of the underlying barriers to immune responses in non-inflamed tumors, as well as the requirements for generating an anti-tumor immune response de novo. Doing so will identify strategies to reverse the non-inflamed tumor phenotype and promote tumor control alone or in combination with existing immunotherapies. In addition to evaluating non-inflamed tumors from an immune cell perspective, it will also be beneficial to examine the tumor cell compartment to identify the ways in which they block successful immune infiltration.

The WNT/β-catenin pathway was the first pathway identified to mediate immune exclusion in melanoma through tumor cell-intrinsic oncogene activation[10]. The initial observation was made by segregating TCGA metastatic melanoma patients into T cell-inflamed and non-T cell-inflamed cohorts using an activated T cell gene signature. Further analysis of the RNA sequencing as well as whole exome sequencing data revealed that nearly half of the non-T cell-inflamed cohort displayed increased activation of the pathway[38]. This led to the development of the BPC mouse model with constitutively active β-catenin described in the previous section.

Subsequent analyses in bladder cancer found that WNT/β-catenin pathway activation was frequently associated with lack of T cell inflammation in this tumor type as well[41]. In a TCGA-wide study, overactivation of WNT/β-catenin signaling was found to be present in the non-T cell-inflamed subset of patients in 28 of the 31 tumor types analyzed[42]. This indicates that aberrant activation of the pathway frequently emerges as a conserved mechanism to promote immune exclusion, regardless of tumor type. The mechanism by which WNT/β-catenin activation is thought to mediate immune exclusion is through lack of CCL4 and CCL5 production which results in a lack of $CD103^+$ DC recruitment, although other mechanisms also might be involved as well. Strategies aimed at targeting overactive WNT/β-catenin signaling in tumor cells are being explored but have yet to enter clinical development.

Additional pathways have been identified in various cancers that negatively associate with T cell inflammation. In melanoma, loss of the tumor suppressor PTEN was shown to correlate with non-responsiveness to anti-PD-1 therapy and low levels of tumor-infiltrating T cells[43]. PTEN loss was associated with upregulation of CCL2 and VEGF as well as resistance to T cell-mediated killing through autophagy inhibition. In preclinical models, an anti-VEGF-blocking antibody was able to improve T cell infiltration as well as antitumor activity of T cells against PTEN-deficient tumors. This corroborates the notion that PTEN loss in melanoma helps resist T cell infiltration by producing immune inhibitory cytokines[44,45]. The pro-tumor effects of PTEN loss could also be overcome using a PI3Kβ inhibitor, which sensitized PTEN-null melanomas to in vitro T cell killing, increased in vivo T cell infiltration, and improved tumor control.

Gain of function mutations in IDH1 and IDH2 are extremely common in glioma and occur in 70-80% of tumors[46]. Gliomas with IDH-activating mutations were also found to express

lower levels of T cell-associated genes and genes associated with IFN-γ-inducible chemokines[47]. Mechanistic studies revealed that IDH gain of function activity is mediated through the conversion of α-ketoglutarate to R-2-hydroxyglutarate, which limits intratumoral CXCL9 and CXCL10[48]. As CXCL9 and CXCL10 are key chemokines for recruiting effector T cells to tumors, this mechanism likely explains why IDH-activated gliomas may exhibit reduced levels of T cell infiltration. Interestingly, blocking R-2-hydroxyglutarate production using a selective inhibitor of mutated IDH1 restored chemokine expression, improved T cell infiltration, and increased peptide vaccine efficacy in mouse models of glioma[47].

These examples highlight the fact that tumor-intrinsic mediation of T cell exclusion through oncogenic mutations have the potential to affect different processes upstream of T cell infiltration. In the tumors with altered WNT/β-catenin signaling, lack of chemokines like CCL4 and CCL5 known to recruit $CD103^+$ DCs seems to be a major mechanism impairing generation of an active T cell response. In the cases of PTEN and IDH mutation, tumors appear to block T cell recruitment either by producing factors such as CCL2 and VEGF to inhibit T cell infiltration or by failing to produce the required chemokines CXCL9 and CXCL10.

An encouraging outcome of these studies is the finding that several of these tumor-intrinsic defects can be reversed by targeting the aberrant pathway, resulting in de novo T cell infiltration and improved tumor control. In the case of WNT/β-catenin for which inhibitors have not yet been fully developed, strategies to drive $CD103^+$ DC recruitment directly may provide a viable alternative approach. Regardless, the approach of identifying tumor-intrinsic differences between T cell-inflamed and non-T cell-inflamed human tumors can yield novel targets which, if successfully drugged, might be capable of reversing immune exclusion in patients. These pathways have the potential of being broadly applicable in many tumor types, as in the case of

WNT/β-catenin, or more specific to one or more tumor types, as in the case of glioma IDH mutations.

1.07 Wilms tumor as a severely non-T cell-inflamed cancer type

While the activation of certain genes, such as β-catenin, has been identified to promote the non-inflamed tumor phenotype, tumors may employ as yet unknown mechanisms to impair T cell inflammation. Closer examination of human tumor transcriptional data, especially in pediatric tumors with few antigenic mutations, may uncover additional pathways that drive the non-T cell-inflamed phenotype. Wilms tumor is the most common pediatric kidney malignancy and affects approximately 1 out of every 10,000 children[49,50]. While the characterization of endogenous immune responses to adult tumors has led to the development of successful immunotherapeutic strategies, knowledge of pediatric anti-tumor immunity remains limited. Compared to adult tumors, pediatric tumors tend to have sparse neoantigens as well as an increased degree of stemness, which has been associated with immune cell exclusion and resistance to immune-mediated elimination[51]. Wilms tumors in particular have a limited number of genetic aberrations and patients demonstrate a reduced autoantibody responses compared to neuroblastoma patients, which indicates fewer immunogenic antigens are present[52,53]. In the three major adult kidney cancer types, a Tumor Inflammation Signature (TIS) scores predict response to checkpoint blockade immunotherapy, while tumor mutational burden does not[54]. Renal clear cell carcinoma (KIRC) has the second highest TIS among all TCGA adult tumor types and is relatively responsive to immunotherapy without having a particularly high mutation load. On the other hand, chromophobe renal cell carcinoma (KICH) and kidney renal papillary

cell carcinoma (KIRP) have similar mutation loads to KIRC, but lower TIS scores and appear to show lower responsiveness to PD-1 blockade.

The most commonly mutated gene in Wilms tumor is *CTNNB1*, and other recurring mutations also promote Wnt pathway activation[55,56]. Interestingly, as mentioned above, active β-catenin signaling associates with immune exclusion across adult tumors and mechanistically promotes T cell exclusion in mouse melanoma models[38,57]. Due to these and other factors, one might expect Wilms tumors to be relatively non-inflamed. While some studies with limited numbers of patients have reported on the presence of T and NK cells in Wilms tumors[58–60], others have observed low PD-L1 expression, which may indicate sparse T cell infiltration[61,62]. Additionally, Wilms tumors with lower $CD8^+$ TIL scores are associated with larger size, increased invasiveness and metastasis, and shorter overall patient survival[63]. These results suggest that when T cell inflammation does occur in Wilms tumors, it can be associated with improved prognosis. A deeper characterization of pediatric tumors, especially those with low mutation burden and low T cell inflammation, may shed light on tumor-intrinsic mechanisms of immune evasion relevant to adult tumors as well.

Chapter 2: Materials and Methods

2.01 Cell lines and culture conditions

Macrophage and tumor cell lines were passaged in DMEM (Fisher #11995073) supplemented with 10% heat-inactivated fetal bovine serum, 100 U/mL Penicillin/Streptomycin (Fisher 15140122), and 1% Non-Essential Amino Acids (Fisher #11140050). Wild type (WT) mouse macrophages were immortalized as described in Roberson and Walker[64] and were obtained from the laboratory of Dr. K. Fitzgerald at the University of Massachusetts. $Asc^{-/-}$ macrophages that overexpress STING-HA tag were used to measure STING aggregation. To measure NF-κB activity in reporter macrophages, RAW-Blue™ Cells were used (Invivogen raw-sp). The B16.F10.SIY (henceforth referred to as B16.SIY) melanoma cell line was derived from C57BL/6 mice as described[65]. The DC2.4 dendritic cell line was purchased from Sigma (#SCC142) and cultured in RPMI (Fisher #11875119) supplemented with 10% heat-inactivated fetal bovine serum, 1% L-Glutamine (Fisher #25030081), 1% Non-Essential Amino Acids (Fisher #1140050), 1% HEPES Buffer Solution (Fisher #15630080), and 0.0054% β-Mercaptoethanol (Fisher #21985023).

2.02 In vitro stimulation assays

Cells were seeded in tissue culture-treated 6 well plates at a density of 1 million cells per well. The next day cells were stimulated with one of several agonists depending on the experiment. DMXAA (Cayman Chemical #117570-53-3) and LPS (Cell Signaling #14011)

stimulations were performed at 50 μg/mL and 50 ng/mL, respectively, unless otherwise noted. Cells were stimulated for 2 hours at 37° C prior to fixation or lysis, depending on the experiment.

2.03 Quantitative real-time PCR

RNA was extracted from stimulated cells using the Qiagen RNeasy Micro Kit according to the manufacturer's protocol. Columns were substituted with EconoSpin All-in-one silica membrane mini spin columns (Epoch Life Science). Following isolation, RNA concentration was quantified by nanodrop and diluted to 1.5 μg per reaction with water. RNA was treated with DNAse I (Sigma #4716728001) prior to cDNA synthesis using high-capacity reverse transcriptase (Fisher #4368814). The resulting cDNA was resuspended with water to a final volume of 100 μL, 5 μL of which was used for each qRT-PCR reaction with 20 μL of Taqman gene expression master mix (Fisher #4369514). Roche probes and primers were added to the master mix as described below, and samples were run on a StepOne Plus real-time PCR machine (Applied Biosystems #4376600).

Table 2.1. Mouse qRT-PCR primers

Target	Roche Probe	Name	Sequence
IFN-β	#108	IFN-β-F	ggaaagattgacgtgggaga
		IFN-β-R	cctttgcaccctccagtaat
GAPDH	#9	GAPDH-F	agcttgtcatcaacgggaag
		GAPDH-R	ttgatgttagtggggtctcg

2.04 Immunofluorescent imaging Flow Cytometry

Macrophages were stimulated at a minimum of 2 million cells per condition. STING aggregation was measured in STING-HA tagged macrophages, whereas IRF3 and p65 nuclear

translocation was measured in WT macrophages. Following stimulation, cells were washed with PBS and resuspended in fixation/permeabilization buffer from a kit (Fisher #00552300). The below antibodies were used in intracellular staining for the antigens of interest.

Table 2.2 Immunofluorescent imaging antibodies

Antigen	Vendor	Catalog	Specificity	Isotype
HA tag	Cell Signaling	3724	All	Rabbit
IRF3	Cell Signaling	4302	Hu, Mu	Rabbit
p65	Cell Signaling	8242	Hu, Mu	Rabbit

APC-conjugated goat anti-rabbit secondary antibodies were used for secondary staining. Prior to imaging, samples were stained for 5 minutes with 2 drops per mL DAPI (Akoya #FP1490) in permeabilization buffer to label nuclei and washed twice with PBS. An Amnis ImageStreamX machine was used to acquire images, which were then analyzed using IDEAS software according to the manufacturer's instructions.

2.05 NF-κB reporter assay

NF-κB reporter RAW-Blue^{TM} macrophages were seeded at 50,000 cells per well in a 96 well tissue culture-treated plate. Cells were stimulated the next day with DMXAA, LPS, or both at a range of doses for two hours. Cell suspensions were incubated with QUANTI-Blue^{TM} according to manufacturer's instructions and SEAP levels were measured using a spectrophotometer at 650 nm.

2.06 Ex vivo stimulation

Spleens from RelA$^{fl/fl}$ x CD11c-Cre mice (Jax 024342 crossed to Jax 008068) were harvested and incubated with digestion buffer for 30 minutes at 37^{o} C while shaking at 200

RPM. The digestion buffer contained RPMI (Fisher #11875119), 2% fetal bovine serum, 200 units/mL bovine pancreas Deoxyribonuclease I (Sigma C5138), 1 mg/mL Hyaluronidase (Sigma H6254), and 1 mg/mL Collagenase Type IV (Sigma C5138). Digested spleens were then mashed through a 70 μm cell strainer and washed with 15 mL PBS. Gey's solution (500 mL water with 4.15 g NH_4Cl plus 0.5 g $KHCO_3$ and filter sterilized) was added for 1 minute to lyse red blood cells in the mixture. $CD11c^+$ cells were isolated using the CD11c MicroBeads UltraPure kit using LS columns from Miltenyi (#130125835) according to manufacturer's instructions. Purified cells from each spleen were resuspended in complete DMEM, divided into four groups, and stimulated for two hours with the conditions control, LPS, DMXAA, or LPS+DMXAA. Following stimulation, qRT-PCR for IFN-β and GAPDH was performed. Cre-negative spleens from littermate control mice were used as controls. Approximately $1/50^{th}$ of each sample was removed following CD11c isolation to check the cellular purity by flow cytometry, and only samples containing 5% or fewer of T, B, and NK cells were used. The flow cytometry panel used is described below.

Table 2.3 Flow cytometry antibodies to assess CD11c purity

Marker	Clone	Fluorophore	Vendor
B220	RA3-6B2	FITC	PharMingen
CD11b	M1/70	BV711	BioLegend
CD11c	N418	PE	BioLegend
CD3	17A2	AF700	BioLegend
CD45	30-F11	APC-Cy7	BioLegend
I-A/I-E	M5/114.15.2	PacBlue	BioLegend
GR-1	RB6-8C5	PE-Cy7	BioLegend
Viability	Fixable Viability Dye eFluor™ 506		eBioscience

2.07 Transplantable tumor model

C57BL/6 obtained from Taconic Biosciences (Hudson, NY) were housed in specific pathogen-free (SPF) conditions. TLR4 knockout (Jax 029015) and STING knockout (Jax 025805) mice were also housed in SPF conditions. Mice were given 1 million live B16.SIY tumor cells at 6-8 weeks of age via subcutaneous injection. Tumor volume was calculated by tumor length x width x height as measured with calipers three times per week until endpoint size was reached.

2.08 Genetically engineered mouse (GEM) tumor model

BPC mice were generated by crossing Tyr:Cre-ER (provided by L. Chin) mice to LSL-$Braf_{V600E}$ mice (provided by M. MacMahon) to $Pten_{fl/fl}$ mice (provided by T. Mak) to LSL-CAT-STA mice (provided by F. Gounari). BPC-SIY mice had an additional cross to Rosa26-LSL-SIY mice (Jax strain 009044). At 6-10 weeks of age, tumors were induced by applying 5 µL of 4-OH-tamoxifen (Sigma #H7904) dissolved at 10 mg/mL in 100% ethanol to the shaved backs of mice. Tumor measurements and treatments began four weeks post tumor induction. Tumor volume was calculated by tumor length x width x height as measured with calipers three times per week until endpoint size was reached.

2.09 In vivo agonist and antibody treatment

In vivo DMXAA injections were performed intratumorally with a single dose of 250 µg in 50 µL per mouse unless otherwise specified. In vivo LPS injections were performed

intratumorally with a single dose of 250 ng in 50 µL per mouse unless otherwise specified. Both LPS and DMXAA were injected on day 11 post tumor inoculation.

For immunotherapy experiments in BPC mice, a combination of anti-PD-L1 (BioXCell #BE0101) and anti-CTLA-4 (BioXCell #BE0131) monoclonal antibodies was used. The antibodies were injected intraperitoneally at a dose of 100 µg in 100 µL. Antibody injections began at 4 weeks post tumor induction or 5 days post DMXAA injection when used and were administered 3 times per week. Flt3L injections in BPC mice were intratumoral and performed at 4 weeks post tumor induction, as a single dose of 50 µg in 50 µL unless otherwise specified. DMXAA injections in BPC mice were single injections of 500 µg in 50 µL and were administered at 4 weeks post tumor induction or 5 days post Flt3L injection when applicable.

For experiments involving $CD8^+$ T cell depletion, mice received intraperitoneal injections of anti-CD8 monoclonal antibody (BioXCell #BE0223) dosed at 200 µg in 100 µL. $CD8^+$ T cell depletion injections were done weekly starting at the first dose of anti-PD-L1 + anti-CTLA-4. Blood samples were drawn, and flow cytometry was performed with the following panel to confirm the depletion.

Table 2.4 Flow cytometry antibodies to assess $CD8^+$ T cell depletion

Marker	Clone	Fluorophore	Vendor
CD11b	M1/70	AF488	BioLegend
CD11c	N418	BV605	BioLegend
CD3	17A2	BV711	BioLegend
CD4	GK1.5	APC-Cy7	BioLegend
CD45	30-F11	PB	BioLegend
CD8	53-6.7	PE-Cy7	eBioscience
I-A/I-E	M5/114.15.2	AF700	eBioscience
Viability	Fixable Viability Dye eFluor™ 506		eBioscience

2.10 Tissue processing and immune cell isolation

For the B16.SIY transplantable model, tumors were dissected and weighed prior to digestion for 30 minutes at 37° C in tumor digestion buffer while shaking at 200 RPM. The digestion buffer contained RPMI (Fisher #11875119), 2% fetal bovine serum, 200 units/mL bovine pancreas Deoxyribonuclease I (Sigma C5138), 1 mg/mL Hyaluronidase (Sigma H6254), and 1 mg/mL Collagenase Type IV (Sigma C5138). Digested tumors were mashed through a 70 μm cell strainer and washed twice with 40 mL of PBS. Following the second wash, tumor cells were resuspended in 8 mL of PBS. Next, 3 mL of Ficoll-Hypaque (Fisher #17144003) was layered under the cell suspension to enrich for immune cells within the tumor mixture. Following a 30-minute centrifugation at 400x*g*, the buffy layer was taken and washed with FACS buffer (10% FBS, 1 mM EDTA in PBS) prior to antibody staining.

2.11 Flow cytometry of tumor-infiltrating immune cells

Cells were first stained with PE-MHC class I pentamer which contained murine H-2Kb complexed to SIYRYYGL peptide (Proimmune) and purified CD16/32 to block non-specific Fc R II/III binding. This step was performed in Brilliant Stain Buffer Plus (Fisher #566385) diluted in FACS buffer for 30 minutes at room temperature. The remaining surface antibodies in FACS buffer were added for an additional 30 minutes at room temperature. Cells were then fixed and permeabilized with the Foxp3 / Transcription Factor Staining Buffer Set (Fisher #00-5523-00) for 30 minutes at room temperature and washed with 1X Permeabilization Buffer from the set. Cells were incubated overnight at 4° C with the intracellular antibodies in 1X Permeabilization Buffer. The next day, cells were washed three times with 1X Permeabilization buffer and resuspended in 150 μL FACS buffer prior to flow cytometry. Samples were run on a Cytek™

Aurora® cytometer with SpectroFlo software. FlowJo software (Tree Star) was used for data analysis.

Table 2.5 Flow cytometry antibodies to assess tumor immune infiltrates

Marker	Clone	Fluorophore	Vendor
CD103	2E7	BV421	BioLegend
CD11b	M1/70	BV570	BioLegend
CD11c	N418	AF647	BioLegend
CD19	6D5	BV510	BioLegend
CD206	C068C2	BV605	BioLegend
CD3	17A2	AF700	BioLegend
CD4	GK1.5	Spark NIR685	BioLegend
CD44	IM7	FITC	BioLegend
CD45	30-F11	AF532	BioLegend
CD62L	MEL-14	PE-Cy7	BioLegend
CD69	H1.2F3	BUV563	BD Biosciences
CD80	16-10A1	PE/Dazzle594	BioLegend
CD86	PO3	BUV496	BD Biosciences
CD8a	53-5.7	PerCP ef710	eBioscience
F4/80	BM8	PerCP/Cy5.5	BioLegend
Foxp3	FJK-16a	APC	BioLegend
I-A/I-E	M5/114.15.2	Pacific Blue	BioLegend
Ki67	B56	BV711	BD Biosciences
Ly6C	HK1.4	BV785	BioLegend
Ly6G	1A8	BUV661	BD Biosciences
NK1.1	PK136	APC-Cy7	BioLegend
PD-1	J43	BUV395	BD Biosciences
PDCA-1	927	BV650	BioLegend
Viability	Zombie NIR™ Fixable Viability Kit		BioLegend

2.12 Immunofluorescence of human tissue samples

5-µm cut sections from formalin-fixed paraffin embedded (FFPE) blocks were stained using Opal multiplex kit (AKOYA Bioscience, Menlo Park, CA, USA) according to the manufacturer's instructions. Briefly, slides were baked for 1 h at 60°C. After deparaffinization and rehydration, tissues were fixed with 10% neutral buffered formalin. Antigen retrieval was performed with pH 9 buffer for 20 minutes at 110℃ in a pressure cooker followed by blocking.

Tissues were then incubated with each primary antibody for 1 hour at room temperature (MSH2 [D24B5, 1:200], CD8 [M7103], SOX10 [20B7]), followed by a horseradish peroxidase-conjugated secondary antibody for 10 minutes at room temperature. Signal amplification was achieved by the corresponding Opal fluorophore (AKOYA Bioscience, Menlo Park, CA, USA) reaction utilized tyramide signal amplification for 10 minutes at room temperature. The process from antigen retrieval to signal amplification was repeated for each of the target molecules. After staining all the target molecules, slides were counterstained with 4', 6-diamidino-2-phenylindole (DAPI) and were mounted and coverslipped.

2.13 Multispectral scanning and image analysis

The stained slides were imaged using the Vectra® Polaris™ Automated Quantitative Pathology Imaging System (AKOYA Bioscience, Menlo Park, CA, USA) at 20x resolutions with the following channels: DAPI, FITC, Cy3, Texas red and Cy5. On each scanned image, five regions of interest (ROI) of preset size that had the most abundant $CD8^+$ cell infiltration were selected in tumor nests. Those selected ROIs were scanned at 20x resolutions to make .im3 format image files for the following image analysis.

The scanned .im3 format image files were analyzed using inForm® Cell Analysis software (AKOYA Bioscience, Menlo Park, CA, USA). Tissue segmentation was performed by highlighting examples of $SOX10^+$ tumor area, $SOX10^-$ stromal area, and non-cellular area, and allowing the algorithm to learn each tissue type. Cell segmentation was performed using DAPI counterstain, and x and y position was assigned to each cell. The following cell phenotypes were determined by highlighting examples of each cell phenotype and allowing the algorithm to learn each cell phenotype: $SOX10^+$, $CD8^+$, $MSH2^+$, and others. Finally, batch analysis using the

trained algorithm was performed for all the ROIs, outputting information including tissue area and phenotype of each cell. The numbers of each immune cell phenotype were calculated as the numbers in tumor areas divided by the number of the total cells in tumor areas.

2.14 Analysis of RNA sequencing data

RNA sequencing data were downloaded from the Genomic Data Commons for adult TCGA samples and the Therapeutically Applicable Research to Generate Effective Treatments (TARGET) database for pediatric samples. Raw read counts were processed by TMM normalization followed by log2 transformation. Differential gene expression analysis was performed using the limma voom package in R. Pathways significantly altered by the differentially expressed genes were detected using Ingenuity Pathway Analysis (IPA) from Qiagen Inc using the curated Ingenuity Knowledge Base. Tumor Inflammation Signatures (TIS) were calculated as the median of normalized log2-expression of the following 18 genes: PSMB10, HLA-DQA1, HLA-DRB1, CMKLR1, HLA-E, NKG7, CD8A, CCL5, CXCL9, CD27, CXCR6, IDO1, STAT1, TIGIT, LAG3, CD274, PDCD1LG2, CD276.

2.15 Statistical analysis

Tumor growth curves were analyzed in GraphPad PRISM. Differences in growth were determined using Tukey's multiple comparisons post-test. For other comparisons between two groups, unpaired, two-tailed Student's tests were used. For comparisons between three or more groups, one-way ANOVA's were used to evaluate differences, with Benjamini-Hochberg FDR correction for multiple comparisons[66]. Statistical significance was considered to be $p < 0.05$ and

was denoted as follows: *$p < 0.05$, **$p < 0.01$, ***$p < 0.001$, ****$p < 0.0001$. All statistical tests were performed using GraphPad PRISM and R.

Chapter 3: TLR4 agonist LPS augments STING-induced innate immune activation

3.01 Introduction

Pharmacological engagement of the STING pathway has shown great efficacy in preclinical mouse models, but therapeutic effects in human cancer patients have been limited. STING agonists alone may result in suboptimal innate immune activation, which could explain why many patients do not respond to STING agonist therapy. In the context of pathogen exposure, innate immune sensing rarely occurs by activating only one signaling pathway, and mammalian organisms have evolved multiple discrete innate immune sensing receptor systems, leading to the downstream activation of several transcription factors. In the tumor context, IFN-β has been identified as necessary for tumor-specific T cell priming. The IFN-β enhancer contains binding sites for multiple transcription factors, and it is likely that engaging more than one signaling pathway and downstream transcription factor is necessary for optimal IFN-β transcription. We hypothesize that activating multiple signaling pathways may improve innate immune activation in response to tumors and may increase the therapeutic effects of STING agonist therapy.

3.02 LPS synergizes with DMXAA in vitro

We initially examined several TLR agonists, including Pam3CSK4 (TLR1/2), Poly:IC (TLR3), LPS (TLR4), Gardiquimod (TLR7), and CpG ODN1668 (TLR9) for their ability to induce IFN-β transcription in macrophages. Each TLR agonist tested individually at a range of concentrations induced far less IFN-β production than the STING agonist DMXAA (Figure

3.1A). However, when tested in combination with DMXAA, LPS induced a synergistic increase in IFN-β transcription, which was significantly greater than the sum of induction by either agonist alone (Figure 3.1B). This was true across a range of doses tested, and LPS significantly increased the amount of IFN-β produced in response to low doses of DMXAA (Figure 3.1C). The same effect was observed in the DC2.4 cell line, indicating that the synergy observed is not a macrophage-restricted phenomenon but also occurs in DCs (Figure 3.1D).

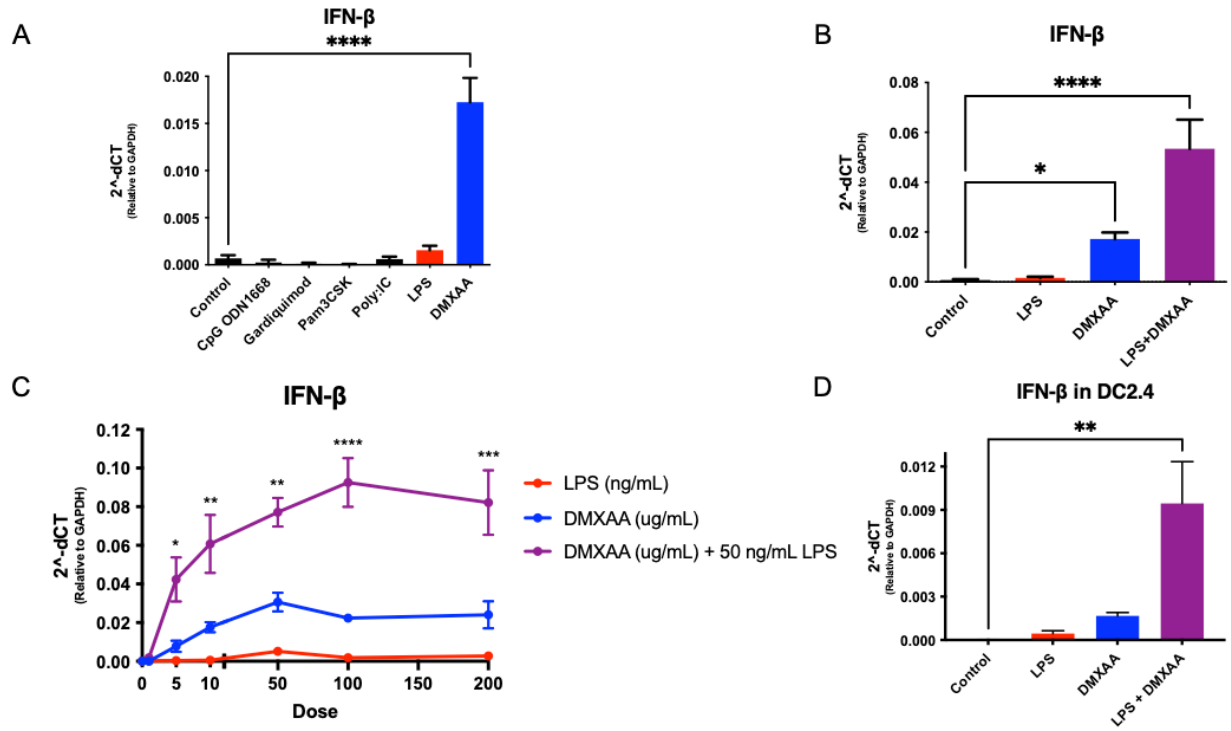

Figure 3.1 LPS and STING agonist DMXAA synergize to induce IFN-β transcription. (A) IFN-β transcription following stimulation of macrophages in vitro with TLR agonists CpG ODN 1668, Gardiquimod, Pam3CSK, Poly:IC, LPS, and STING agonist DMXAA. (B) IFN-β transcription following stimulation of macrophages in vitro with LPS, DMXAA, or combination. (C) IFN-β transcription following stimulation of macrophages in vitro with dose titrations of LPS, DMXAA, or DMXAA + 50 ng/mL LPS. (D) IFN-β transcription following stimulation of DC2.4 cells in vitro with LPS, DMXAA, or combination.

Thus, LPS was able to significantly increase the maximal amount of IFN-β produced in response to DMXAA. Even low doses of DMXAA combined with LPS induced greater IFN-β than high doses of DMXAA alone.

3.03 LPS does not augment DMXAA signaling through STING or IRF3 activation

Next, we sought to determine the mechanism by which the synergy between LPS and DMXAA was occurring, and first focused on the core STING pathway itself. Downstream signaling following STING engagement is well-characterized, and involves STING aggregation followed by TBK1 and IRF3 phosphorylation. This then leads to IRF3 nuclear translocation where it can carry out its transcriptional activity and induce IFN-β production. To assess STING aggregation in response to DMXAA, LPS, and the combination, we stimulated STING-HA labeled macrophages and performed ImageStream analysis to visualize STING aggregation. Robust STING activation was induced by DMXAA and was also present in the LPS+DMXAA condition, but not in the condition with LPS alone (Figure 3.2A, Figure 3.2B). Similarly, LPS did not significantly induce IRF3 nuclear translocation or increase the nuclear translocation induced by DMXAA alone (Figure 3.2C, Figure 3.2D).

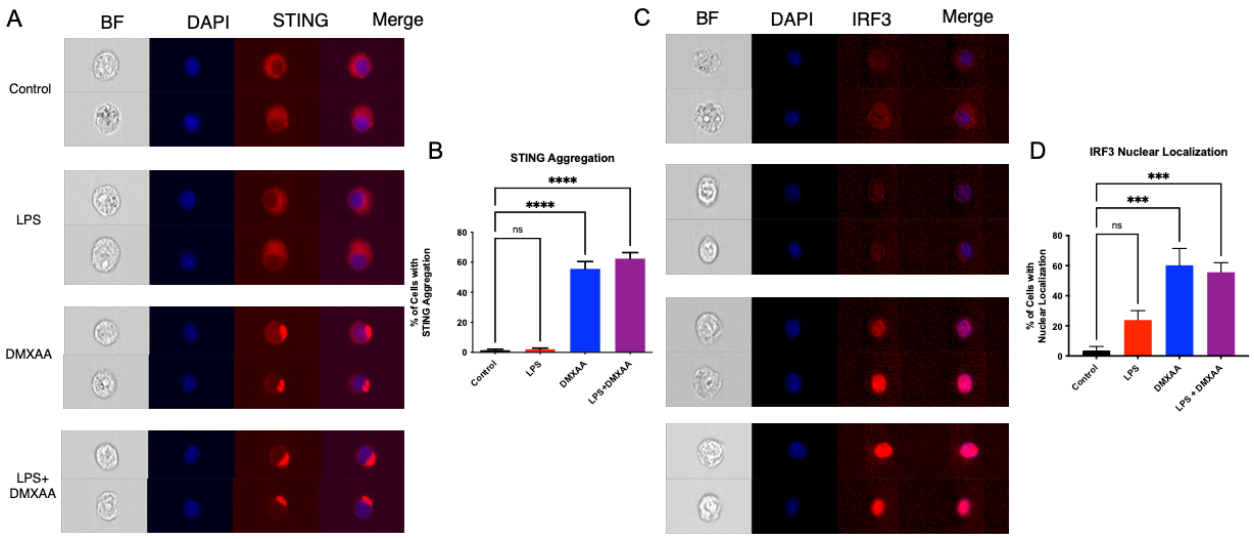

Figure 3.2 LPS does not strongly affect STING aggregation or IRF3 nuclear translocation. (A) ImageStream images of STING aggregation in STING-HA macrophages stimulated with LPS, DMXAA, LPS + DMXAA. (B) Quantification of percentage of cells with STING aggregation following stimulation. (C) ImageStream images of IRF3 nuclear localization in macrophages stimulated with LPS, DMXAA, LPS + DMXAA. (D) Quantification of percentage of cells with nuclear localization based on overlap with DAPI.

These data suggest that LPS is not augmenting the IFN-β response to DMXAA by affecting STING directly or the transcription factor IRF3.

3.04 LPS signaling through NFκB is required for synergy

Since signaling downstream of LPS is known to activate NFκB, and NFκB can contribute to transcriptional regulation of the IFN-β promoter/enhancer, we next examined NFκB in response to stimulation with these agonists. To study NFκB activity, we used ImageStream to measure nuclear translocation of the NFκB subunit p65. Although LPS failed to induce IRF3 nuclear translocation, LPS induced robust p65 nuclear translocation (Figure 3.3A, Figure 3.3B). DMXAA had a relatively minor effect on p65 nuclear translocation, and the combination of LPS

+ DMXAA appeared similar to LPS alone. Next, we examined NFκB activity directly using RAW-Blue^{TM} reporter macrophages. Across a range of doses, LPS induced significantly greater reporter activity than did DMXAA, and the LPS + DMXAA condition appeared similar to LPS alone (Figure 3.3C).

Since NFκB was readily induced by LPS stimulation, we examined whether it was required for the synergistic induction of IFN-β expression. To test the necessity of NFκB for the synergy between LPS and DMXAA, we isolated CD11c^{+} cells from p65$^{fl/fl}$ mice that were CD11c-Cre^{+} or CD11c-Cre^{-} and measured IFN-β following agonist stimulation. As we had observed previously with macrophages and the DC cell line, CD11c^{+} cells from Cre^{-} mice that had p65 intact showed increased IFN-β transcription with LPS+DMXAA compared to DMXAA stimulation alone. However, with CD11c^{+} cells deleted of p65, no such increased was observed with combination treatment . This result indicates that p65 is necessary for the synergy between LPS and DMXAA in causing increased IFN-β production.

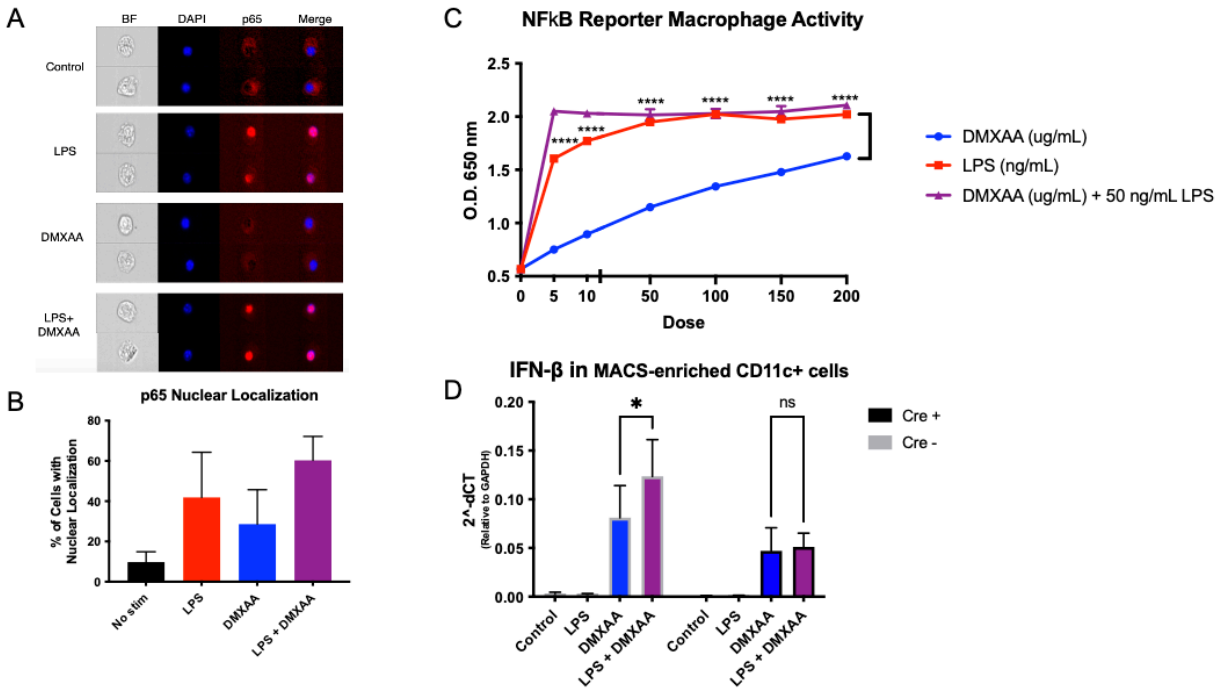

Figure 3.3 LPS promotes NFkB activation by increasing p65 nuclear translocation. (A) ImageStream images of p65 nuclear localization in macrophages stimulated with LPS, DMXAA, LPS + DMXAA. (B) Quantification of percentage of cells with nuclear localization based on overlap with DAPI. (C) NFκB reporter activity in RAW-Blue^{TM} macrophages stimulated with following stimulation with dose titrations of LPS, DMXAA, or DMXAA + 50 ng/mL LPS. (D) IFN-β transcription in CD11c^{+} cells purified from RelA x CD11c-Cre^{+} and RelA x CD11c-Cre^{-} mice stimulated with LPS, DMXAA, LPS + DMXAA.

Overall, these data support our model that DMXAA primarily signals through the transcription factor IRF3, and LPS primarily signals through NFκB. Activation of both of these transcription factors with agonists for both pathways induces synergistic levels of IFN-β transcription.

3.05 LPS synergizes with DMXAA in vivo to promote tumor control

Because LPS + DMXAA induced such a strong IFN-β response in vitro, we next wanted to test if LPS could promote tumor control in vivo with DMXAA. To do so, we used a

suboptimal 250 ug dose of DMXAA, and performed a single intratumoral injection with or without 250 ng LPS. As evidenced by the growth curve, both LPS and DMXAA alone resulted in improved tumor control. However, there was a significant improvement when both agonists were administered together (Figure 3.4).

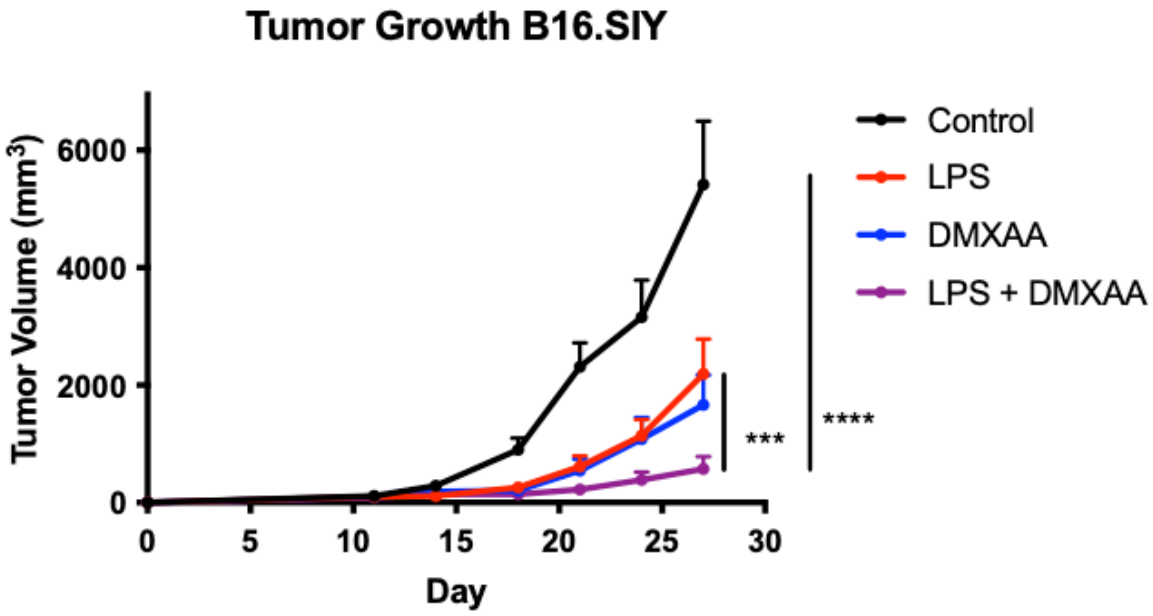

Figure 3.4 Intratumoral LPS improves tumor control alone and in combination with DMXAA.
B16.SIY tumor growth in C57BL/6 mice treated intratumorally on day 11 with 250 µg DMXAA, 250 ng LPS, or both.

This observation indicates that combining agonists for different innate immune pathways, specifically the STING and TLR4 pathways, can result in improved anti-tumor immune responses. To determine whether host expression of STING and TLR4 were required for this improved tumor control, the same in vivo injection strategy was performed in STING$^{-/-}$ and TLR4$^{-/-}$ mice. LPS showed some anti-tumor activity in STING$^{-/-}$ mice, but there was no additional benefit with DMXAA in these mice (Figure 3.5A). Similarly, DMXAA showed some

activity in TLR4$^{-/-}$ mice, but synergy was not observed between the two agonists in these mice either (Figure 3.5B).

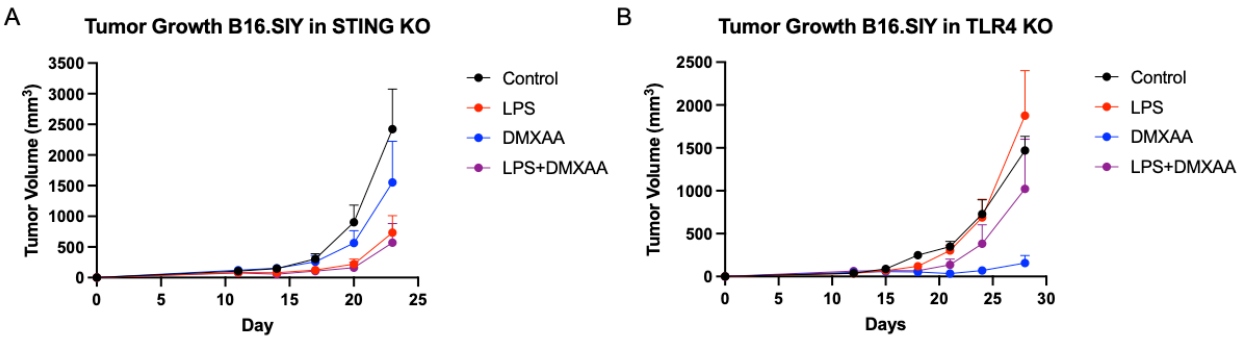

Figure 3.5 In vivo benefit of DMXAA and LPS combination is dependent on STING and TLR4.
(A) B16.SIY tumor growth in STING$^{-/-}$ mice treated intratumorally on day 11 with 250 μg DMXAA, 250 ng LPS, or both. (B) B16.SIY tumor growth in TLR4$^{-/-}$ mice treated intratumorally on day 11 with 250 μg DMXAA, 250 ng LPS, or both.

These data support the notion that host STING signaling and TLR4 signaling must both be intact in order to observe improved tumor control in response to LPS + DMXAA therapy.

3.06 Summary of Findings

By treating APCs with a range of concentrations of STING agonist in addition to TLR agonists, we determined LPS was capable of synergizing with the STING pathway for optimal IFN-β production. We then interrogated downstream signaling events to determine the mechanism driving additional IFN-β production. Based on in vitro experiments performed in macrophages and dendritic cells, DMXAA was found to signal primarily through the transcription factor IRF3, whereas LPS signaled primarily through the transcription factor NFκB. Together, these data suggest a working model that agonists targeting both of these pathways

induce better activation of both IRF3 and NFκB, resulting in augmented IFN-β transcription by innate immune cells and superior tumor control (Figure 3.6).

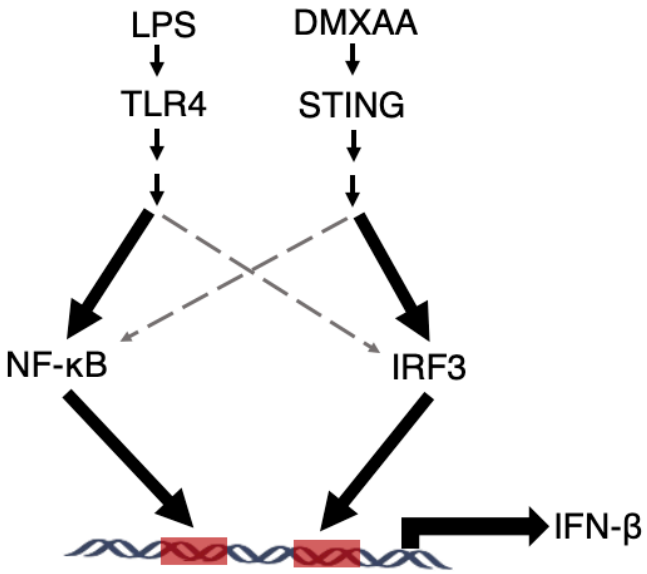

Figure 3.6 Working model of synergy between LPS and DMXAA.
Our current working model that LPS primarily signals through TLR4 to activate the transcription factor NFκB, while DMXAA signaling through STING primarily activates the transcription factor IRF3. When both agonists are present to activate both transcription factors, synergistic levels of are produced IFN-β.

Chapter 4: Flt3L promotes CD103$^+$ DC accumulation in non-T cell-inflamed β-catenin-expresing tumors

4.01 Introduction

STING agonists may be unsuccessful in generating productive T cell responses in non-inflamed tumors because those tumors also lack the required CD103$^+$ DC subset for T cell priming and recruitment. This notion suggests a need to more closely study the non-inflamed tumor microenvironment and understand which innate immune cells and signaling pathways are required for driving tumor-specific T cell priming and recruitment in this context. We postulate that these questions may be addressed using the BRAF-activated, PTEN-deleted, β-catenin-stabilized (BPC) genetic melanoma model. Our laboratory previously showed that tumors induced in these mice lack spontaneous CD103$^+$ DC and T cell infiltration and have low expression of the chemokines known to recruit these cells, namely CCL4 and CXCL9/10. In this way, this model closely resembles the biology of many non-T cell-inflamed human cancers. We hypothesize that recruiting CD103$^+$ DCs to these tumors along with innate immune activation using a STING agonist can lead to the induction of a tumor-specific T cell response and promote tumor control either alone or in combination with checkpoint blockade in this non-T cell-inflamed model.

4.02 DMXAA increases CD8$^+$ T cell but not CD103$^+$ DC infiltration in BPC tumors

Because the STING agonist DMXAA elicited strong anti-tumor responses in the transplantable tumor models tested, we first wanted to determine if the same was also true in the genetic BPC melanoma model. To do so, we performed a dose response for intra-tumoral

DMXAA injections followed by flow cytometry to analyze the immune infiltrate five days post-injection. Injections were done at four weeks post-tumor induction, to allow for treatment of an established tumor. The 500 μg DMXAA injection induced the strongest increase in $CD8^+$ T cells by both number and percentage (Figure 4.1A, Figure 4.1B), however none of the doses tested had an appreciable impact on either the $CD103^+$ DC number and percentage (Figure 4.1C, Figure 4.1D).

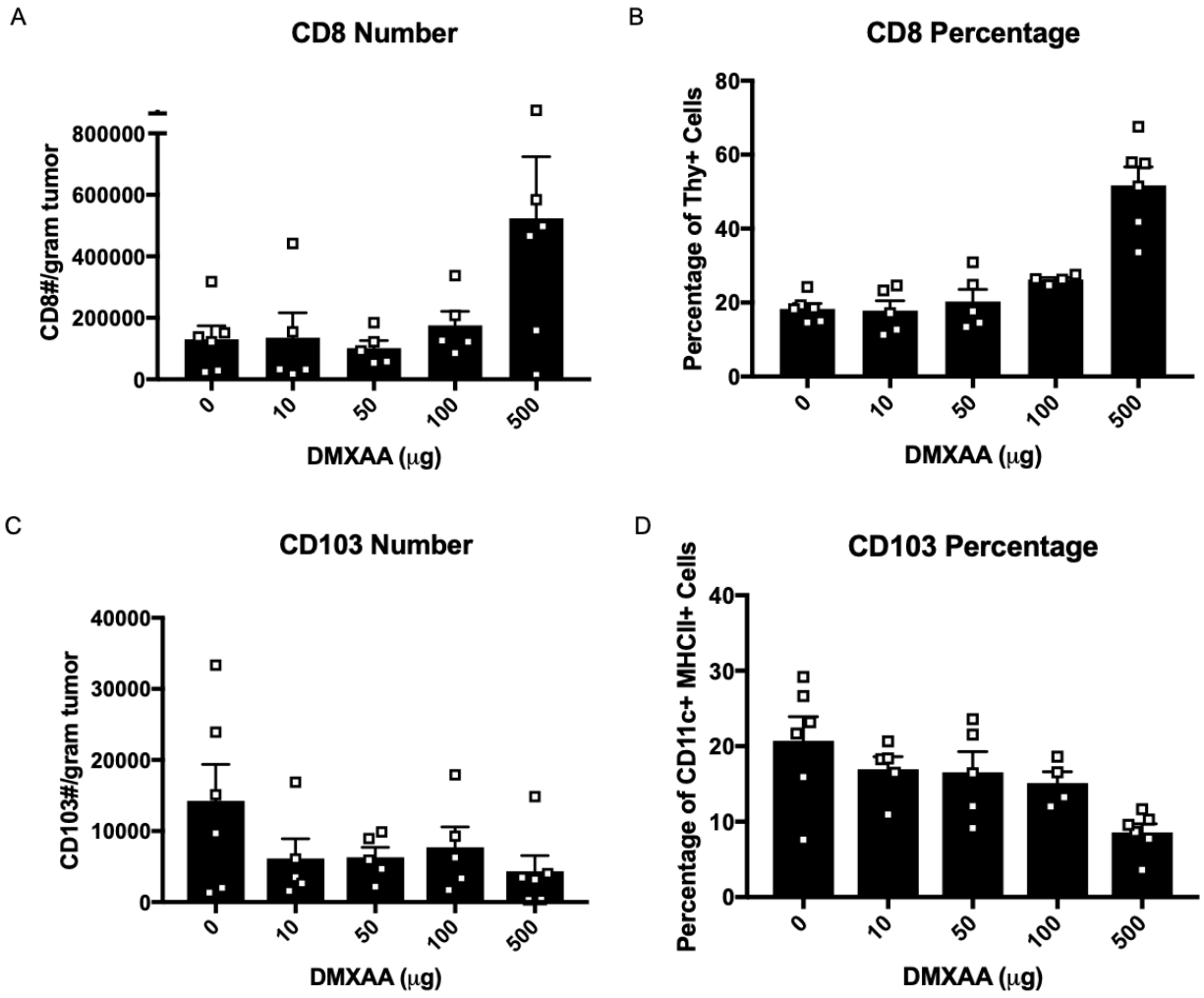

Figure 4.1 DMXAA dose response in BPC tumors
(A) Flow cytometry for $CD8^+$ T cell numbers in BPC tumors five days after DMXAA injection at various doses. (B) Flow cytometry for $CD8^+$ percentage of T cells in BPC tumors five days after DMXAA injection at various doses. (C) Flow cytometry for $CD103^+$ DC numbers in BPC tumors five days after DMXAA injection at various doses. (D) Flow cytometry for $CD103^+$ DC numbers in BPC tumors five days after DMXAA injection at various doses.

Based on these findings, subsequent experiments in this model were performed with the 500 μg intratumoral dose of DMXAA. Additional experiments confirmed that at five days post treatment with DMXAA, there was a significant increase in $CD8^+$ T cells by both number and percentage (Figure 4.2A, Figure 4.2B), but the number and percentage of $CD103^+$ DCs was not significantly altered (Figure 4.2C, Figure 4.2D).

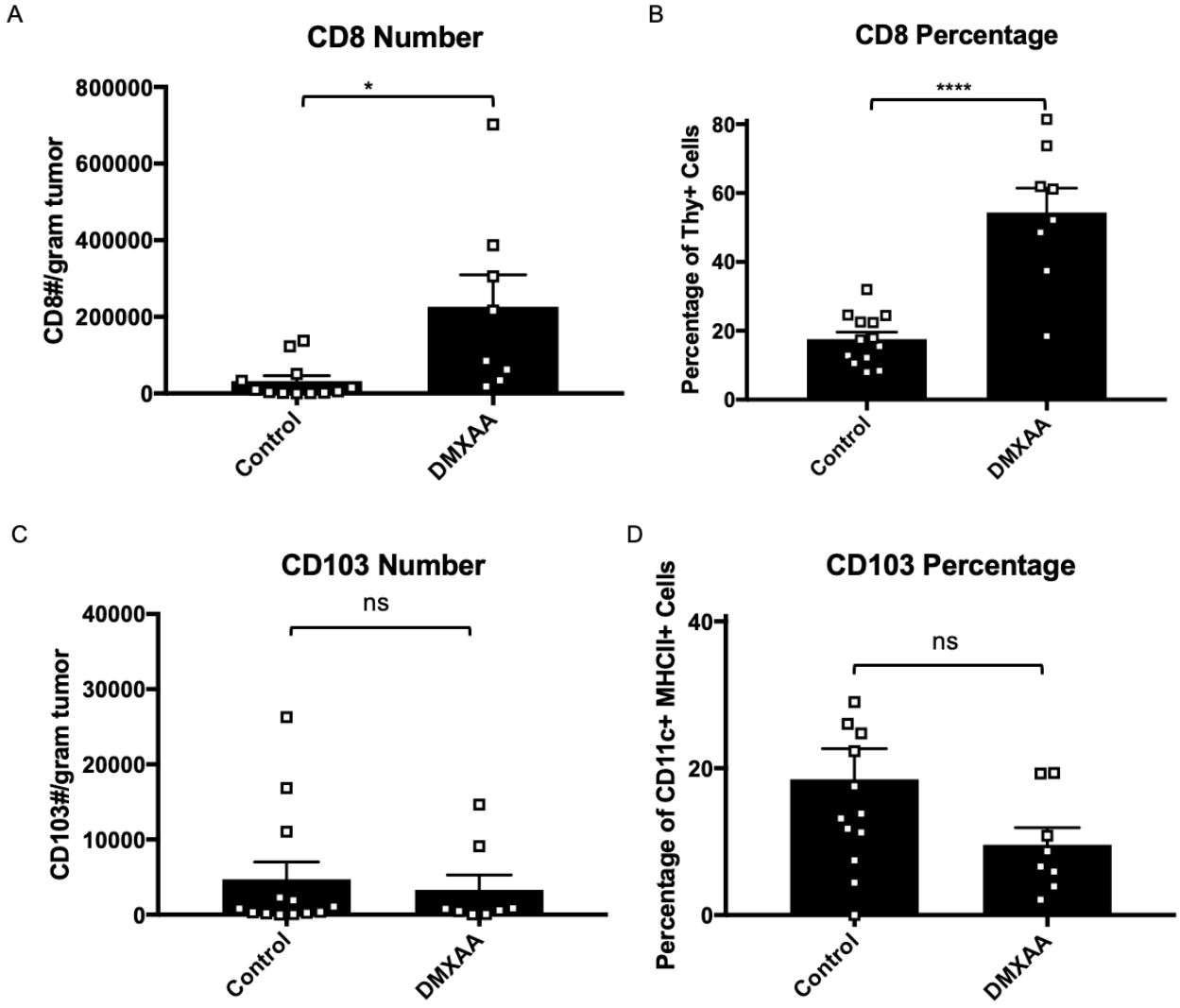

Figure 4.2 DMXAA significantly increases $CD8^+$ T cell numbers but not $CD103^+$ DC numbers

(A) Flow cytometry for $CD8^+$ T cell numbers in BPC tumors five days after DMXAA injection at 500 μg dose. (B) Flow cytometry for $CD8^+$ percentage of T cells in BPC tumors five days after DMXAA injection at 500 μg dose. (C) Flow cytometry for $CD103^+$ DC numbers in BPC tumors five days after DMXAA injection at 500 μg dose. (D) Flow cytometry for $CD103^+$ DC numbers in BPC tumors five days after DMXAA injection at 500 μg dose.

This increase in $CD8^+$ T cell numbers following DMXAA treatment was comparable to the baseline $CD8^+$ T cell infiltration observed in the B16.SIY transplantable model as well as the BP genetic model lacking β-catenin. Since those and other transplantable models respond to checkpoint blockade immunotherapy, it led to the hypothesis that this dose of DMXAA might promote tumor control in the context of checkpoint blockade.

4.03 DMXAA does not sensitize BPC tumors to αPD-L1 + αCTLA-4 immunotherapy

We next sought to determine whether the DMXAA treatment in BPC tumors was able to promote tumor control in vivo, and whether it could sensitize these tumors to checkpoint blockade immunotherapy. To do so, we induced tumors in BPC mice and allowed them to establish for four weeks (Figure 4.3A). At the 4-week timepoint, one intratumoral dose of 500 μg DMXAA was administered, and tumor outgrowth was measured (Figure 4.3B). Unlike what has been observed in transplantable tumor models, DMXAA was unable to lead to tumor control in these mice. Additionally, the combination of DMXAA followed by intraperitoneal anti-PD-L1 + anti-CTLA-4 mAb treatment three times per week was unable to control tumors in this model (Figure 4.3C). While we do not know whether the $CD8^+$ T cells recruited are tumor antigen-specific, these results suggest that accumulation of T cells in the tumor microenvironment without $CD103^+$ DCs is not sufficient to bestow checkpoint blockade therapeutic efficacy.

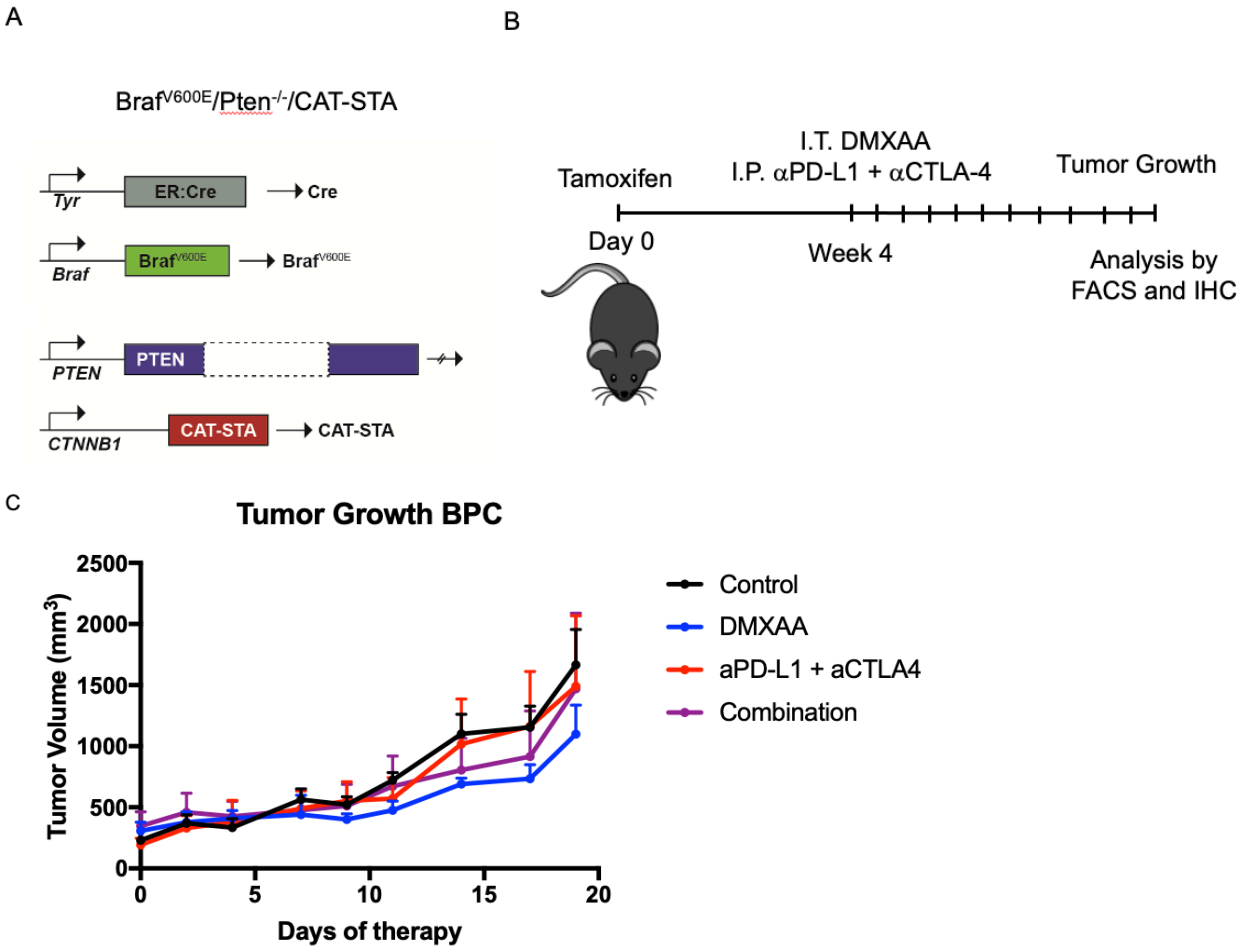

Figure 4.3 DMXAA does not improve BPC tumor control or sensitize to anti-PD-L1 + anti-CTLA-4

(A) Summary of mutations present in BPC tumor model: Tyr:Cre-ER, LSL-$Braf_{V600E}$, $Pten_{fl/fl}$, LSL-CAT-STA. (B) Experimental setup with intratumoral DMXAA injection four weeks post tumor induction and intraperitoneal anti-PD-L1 + anti-CTLA-4 administered three times per week for the remainder of the experiment. (C) Tumor growth curves for BPC mice treated with DMXAA, anti-PD-L1 + anti-CTLA-4, or the combination.

4.04 Flt3L induces CD103$^+$ DC infiltration in BPC tumors

The failure of tumor control with DMXAA treatment alone or in combination with anti-PD-L1 + anti-CTLA-4 may be explained by the lack of recruitment and accumulation of CD103$^+$ DCs. Based on previous work, CD103$^+$ DCs are critical for priming a successful anti-tumor CD8$^+$ T cell response, and also for recruiting and re-activating tumor antigen-specific CD8+ T cells within the tumor site. As such, integrating an additional strategy for CD103+ DC recruitment may be required.

We therefore examined Flt3L as a possible candidate to promote CD103$^+$ DC accumulation in BPC tumors. Flt3L is a hematopoietic growth factor that is known to promote differentiation and proliferation of DCs[67]. A single intratumoral dose was injected at four weeks post-tumor induction, and tumor immune infiltrates were analyzed by flow cytometry five days later. Based on the initial dose response experiments, Flt3L significantly increased the number of CD103$^+$ DCs and CD8$^+$ T cells in these tumors (Figure 4.4A, Figure 4.4C).

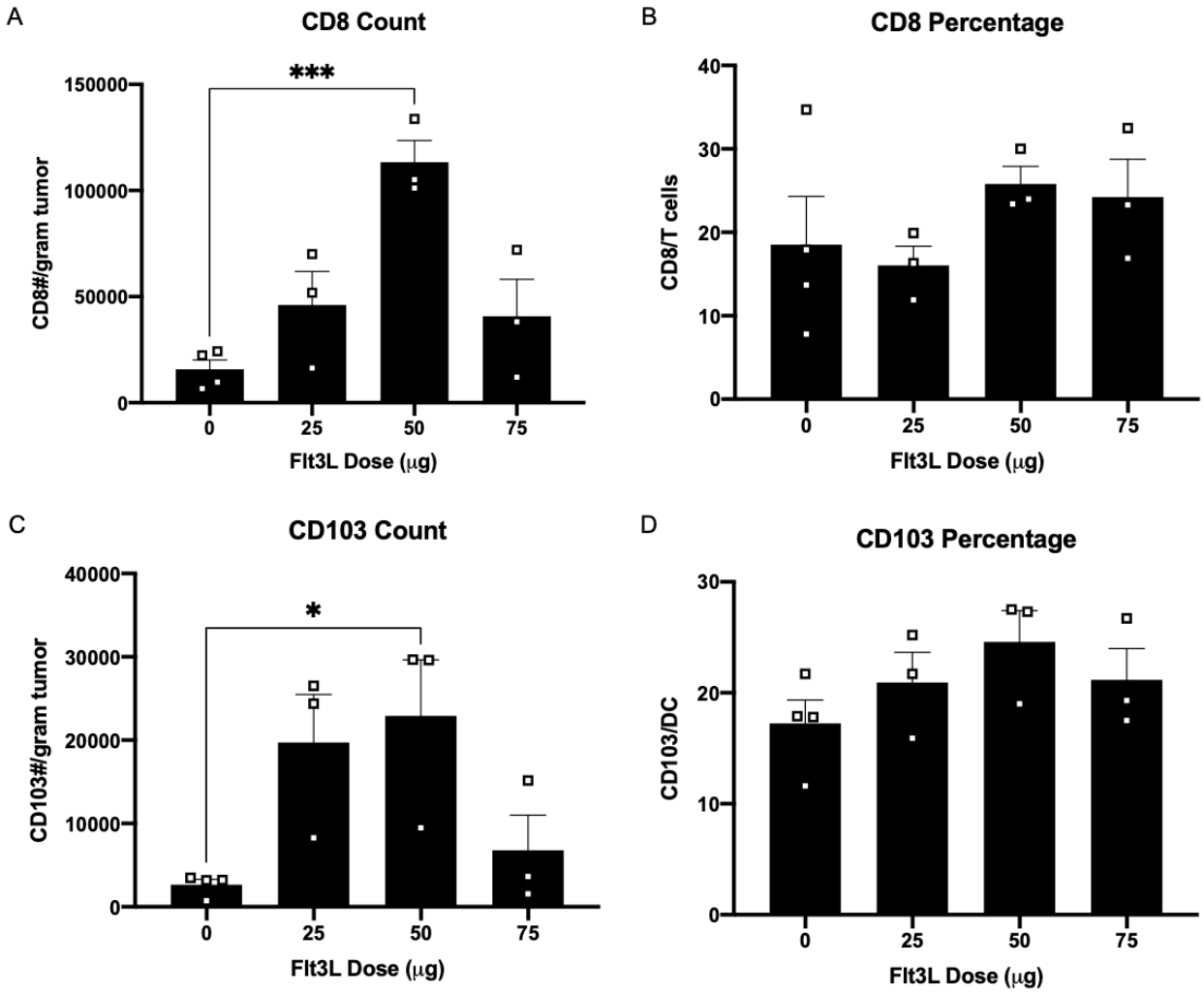

Figure 4.4 Flt3L dose response in BPC tumors
(A) Flow cytometry for $CD8^+$ T cell numbers in BPC tumors five days after Flt3L injection at various doses. (B) Flow cytometry for $CD8^+$ percentage of T cells in BPC tumors five days after Flt3L injection at various doses. (C) Flow cytometry for $CD103^+$ DC numbers in BPC tumors five days after Flt3L injection at various doses. (D) Flow cytometry for $CD103^+$ DC numbers in BPC tumors five days after Flt3L injection at various doses.

4.05 Flt3L + DMXAA does not significantly improve tumor control in BPC mice

To test if Flt3L was able to improve tumor control in BPC mice, a single intratumoral dose was administered and tumor outgrowth was measured. Considering the tumor immunity cycle, $CD103^+$ DCs must be activated in order to prime a successful $CD8^+$ T cell response.

Because it is unclear whether endogenous tumor ligands are sufficient to activate CD103^{+} DCs in this context, we also tested a condition in which DMXAA was administered five days post Flt3L injection (Figure 4.5A). This tested the notion that stimulating newly arrived CD103^{+} DCs in this model with a STING agonist may be sufficient to activate them enough to generate a productive anti-tumor T cell response. However, Flt3L treatment alone, DMXAA treatment alone, and Flt3L followed by DMXAA five days later all did not significantly affect tumor control in BPC mice (Figure 4.5B).

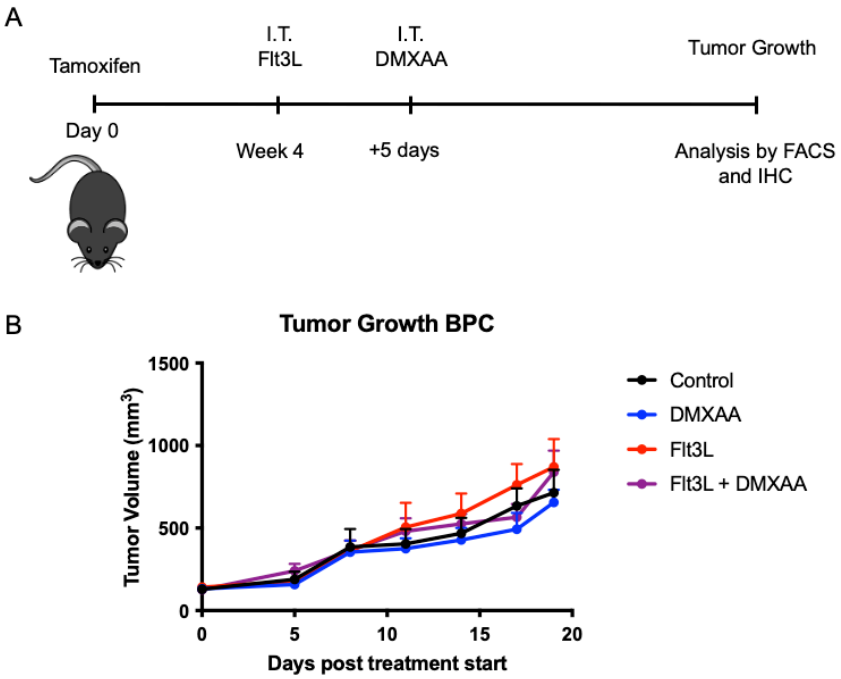

Figure 4.5 Flt3L does not improve BPC tumor control or sensitize to DMXAA therapy
(A) Experimental setup with intratumoral Flt3L injection four weeks post tumor induction and intratumoral DMXAA administered five days later. (C) Tumor growth curves for BPC mice treated with Flt3L, DMXAA, or the combination.

4.06 Flt3L + DMXAA significantly improves tumor control in BPC mice treated with αPD-L1 + αCTLA-4

It was reasoned that generation of a DC and $CD8^+$ T cell infiltrate might not be sufficient for tumor control because of the additional action of the immune checkpoint molecules CTLA-4 and PD-1. Therefore, we administered intratumoral injections of Flt3L with or without DMXAA five days later and injected all four groups with combination anti-PD-L1 + anti CTLA-4 three times per week beginning three days after the DMXAA injection (Figure 4.6A). The Flt3L group and DMXAA group demonstrated modest improvements in tumor control, but strikingly the combination of Flt3L + DMXAA led to significant tumor control in the context of checkpoint blockade antibodies, as evidenced by diminished tumor growth over time and reduced tumor weight at endpoint (Figure 4.6B, Figure 4.6C). Additionally, the combination therapy trended towards an increased number of $CD8^+$ T cells present at endpoint by flow cytometry (Figure 4.6D).

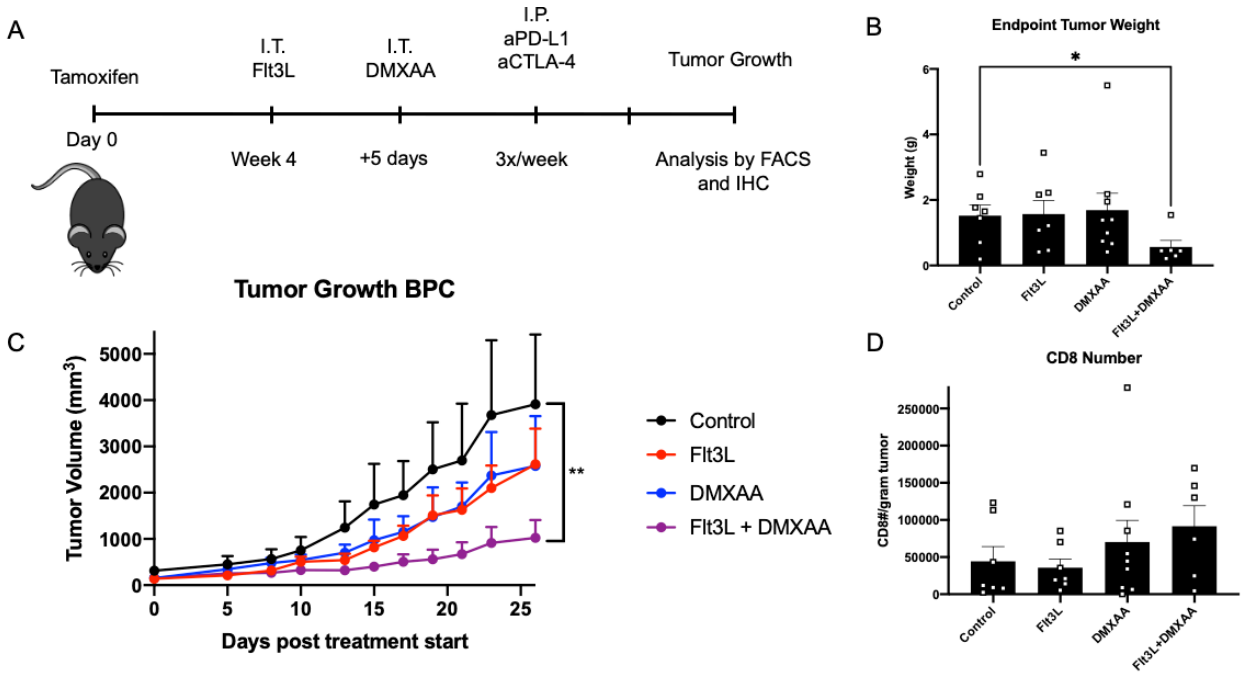

Figure 4.6 Flt3L and DMXAA sensitize tumors to anti-PD-L1 + anti-CTLA-4
(A) Experimental setup with intratumoral Flt3L injection four weeks post tumor induction, intratumoral DMXAA injection five days later, and intraperitoneal anti-PD-L1 + anti-CTLA-4 administered three times per week for the remainder of the experiment. (B) Endpoint tumor weights for BPC mice treated with Flt3L, DMXAA, or the combination. All mice received anti-PD-L1 + anti-CTLA-4. (C) Tumor growth curves for BPC mice treated with Flt3L, DMXAA, or the combination. All mice received anti-PD-L1 + anti-CTLA-4. (D) Number of $CD8^+$ T cells at endpoint by flow cytometry.

Together, these data indicate that to overcome this non-inflamed and difficult-to-treat β-catenin-driven GEM model, it is necessary to recruit $CD103^+$ DCs, activate them, and subsequently support T cell function through checkpoint blockade in order to achieve a therapeutic effect.

4.07 Summary of Findings

Preliminary experiments showed that 500 μg of DMXAA led to significant increases in $CD8^+$ T cells in BPC tumors five days post injection. However, the $CD103^+$ DC numbers in

these tumors were not increased following DMXAA treatment. The T cells recruited following DMXAA treatment were unable to cause tumor control alone or in combination with anti-PD-L1 + anti-CTLA-4. This led us to adopt an additional strategy aimed at promoting $CD103^+$ DC accumulation directly. A single injection of Flt3L was able to drive $CD103^+$ DC accumulation in BPC tumors, with 50 μg being the optimal dose. However, Flt3L alone or with a subsequent DMXAA injection was unable to lead to tumor control in this model. Only when Flt3L and DMXAA were followed by anti-PD-L1 + anti-CTLA-4 was tumor control achieved.

Chapter 5: Low tumor immunogenicity is associated with high DNA repair gene expression

5.01 Introduction

A T cell-rich tumor microenvironment has been associated with improved clinical outcome and better response to immune checkpoint blockade therapies in several adult cancers. Understanding the mechanisms for lack of immune infiltration is critical for expanding immunotherapy efficacy in the clinic. However, much less is known about the tumor microenvironment in pediatric cancers, which harbor a significantly lower tumor mutational burden (TMB) than adult tumors, as well as the molecular mechanisms responsible for driving T cell exclusion in these patients. Wilms tumor is a pediatric kidney cancer type that has been reported to have very low level of T cell infiltration[52]. We reasoned that studying Wilms tumor might reveal novel biologic processes that regulate the degree of immune cell infiltration in the tumor microenvironment. To this end, we analyzed pediatric kidney cancer genomic and clinical data from the Therapeutically Applicable Research to Generate Effective Treatments (TARGET) database.

5.02 Wilms tumor samples demonstrate low T cell inflammation scores

We first aimed to characterize the T cell inflammation status of Wilms tumor samples in the TARGET database using immune gene expression profiling. To do so, we calculated the TIS score for each Wilms tumor sample using a previously defined 18-gene signature designed to measure adaptive anti-tumor immune responses using expression of genes associated with antigen presentation, interferon gamma activity, and cytotoxic cells[54]. We compared TIS scores

from 120 Wilms tumor samples to 149 neuroblastoma samples, 84 osteosarcoma samples, and 65 rhabdoid tumor samples present in the TARGET database. Compared to the other pediatric cancer types tested, Wilms tumor samples had significantly lower TIS scores (Figure 5.1A), suggesting a reduced endogenous anti-tumor immune response. We also examined the Wilms TIS in relation to adult kidney tumors from TCGA, including 538 KIRC samples, 288 KIRP samples, and 65 KICH samples. Among the adult kidney tumor types, KIRC had the highest TIS scores, while KICH had the lowest (Figure 5.1B), which has been previously reported[40]. However, Wilms tumor samples demonstrated significantly lower TIS scores than any of the adult tumor samples including KICH, which is one of the least inflamed tumor types in all of TCGA.

To evaluate whether this was a characteristic of pediatric kidneys being non-T cell-inflamed rather than a feature of Wilms tumors, we next studied the four patients in the TARGET database with paired RNA sequencing for Wilms tumor and adjacent normal kidney tissue. In these patients, the Wilms tumor samples had significantly lower TIS scores than the matched normal samples (Figure 5.1C). Additionally, in a published single cell RNA sequencing dataset[68], Wilms tumors demonstrated a significant reduction in $CD8^+$ T cell percentage when compared to paired normal kidney samples (Figure 5.1D). Therefore, Wilms tumors exhibited lower TIS scores than other pediatric tumor types, other adult kidney tumor types, and matched normal samples, which is supported by less $CD8^+$ T cell infiltration by single cell RNA sequencing in a published dataset.

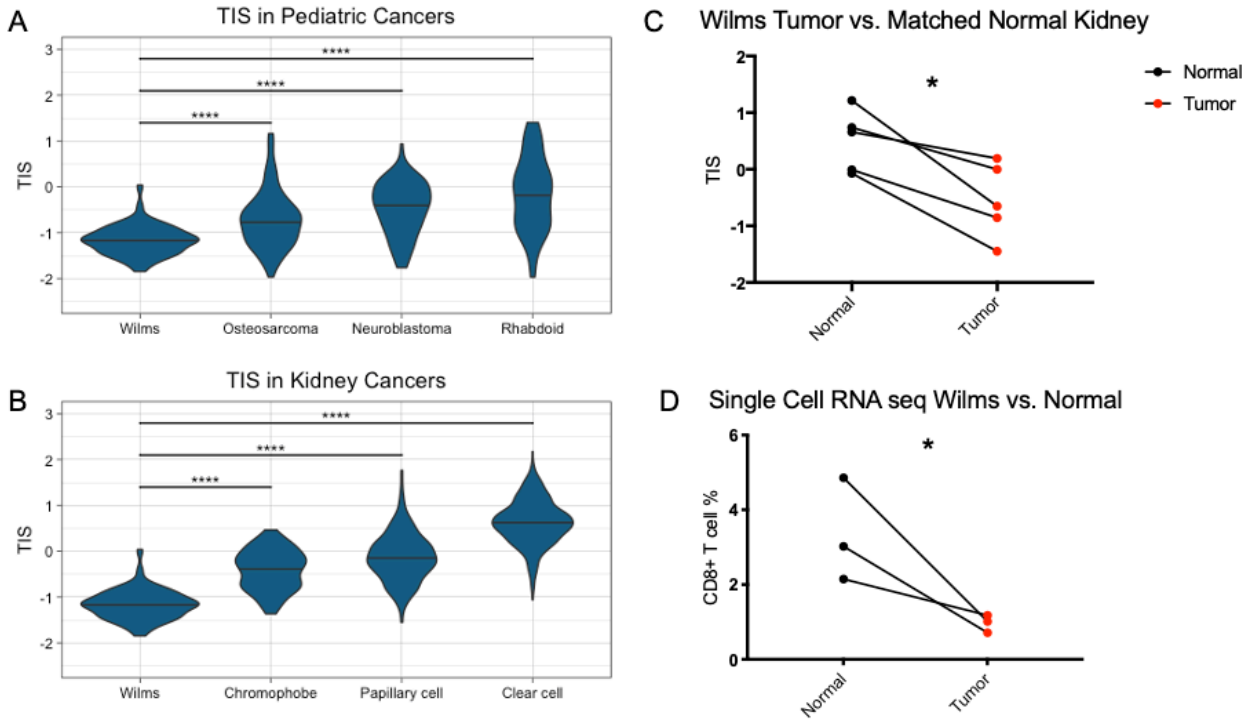

Figure 5.1 Wilms tumors have lower TIS than other pediatric cancer types, adult kidney cancer types, and matched normal kidney samples.
(A) TIS scores in Wilms tumor and the other pediatric tumor types osteosarcoma, neuroblastoma, and rhabdoid tumor. (B) TIS scores in Wilms tumors and the other adult kidney tumor types chromophobe, papillary cell, and clear cell renal carcinoma. (C) TIS scores in Wilms tumor versus matched normal kidney samples. (D) Percentage of $CD8^+$ T cells in Wilms tumor samples by single cell RNA sequencing versus matched normal tissue.

5.03 DNA damage response genes are upregulated in Wilms tumors

To better understand the non-T cell-inflamed Wilms tumor phenotype by gene expression profiling, we used three separate approaches to identify genes that are both upregulated in Wilms tumor and anti-correlated with the TIS. We first identified genes that were differentially expressed and upregulated in Wilms tumor compared to adult kidney cancers. Next, we identified the genes most significantly upregulated in Wilms tumor compared to matched normal tissue. We then determined which genes were most strongly anticorrelated with TIS scores in Wilms tumor samples. The intersection of these three methods identified 496 genes that met our

criteria of being overexpressed in Wilms tumor and negatively associated with T cell inflammation (Figure 5.2A). Interestingly, the top pathways for these genes revealed by Ingenuity Pathway Analysis included several related to DNA damage, cell cycle checkpoint, and DNA repair (Figure 5.2B).

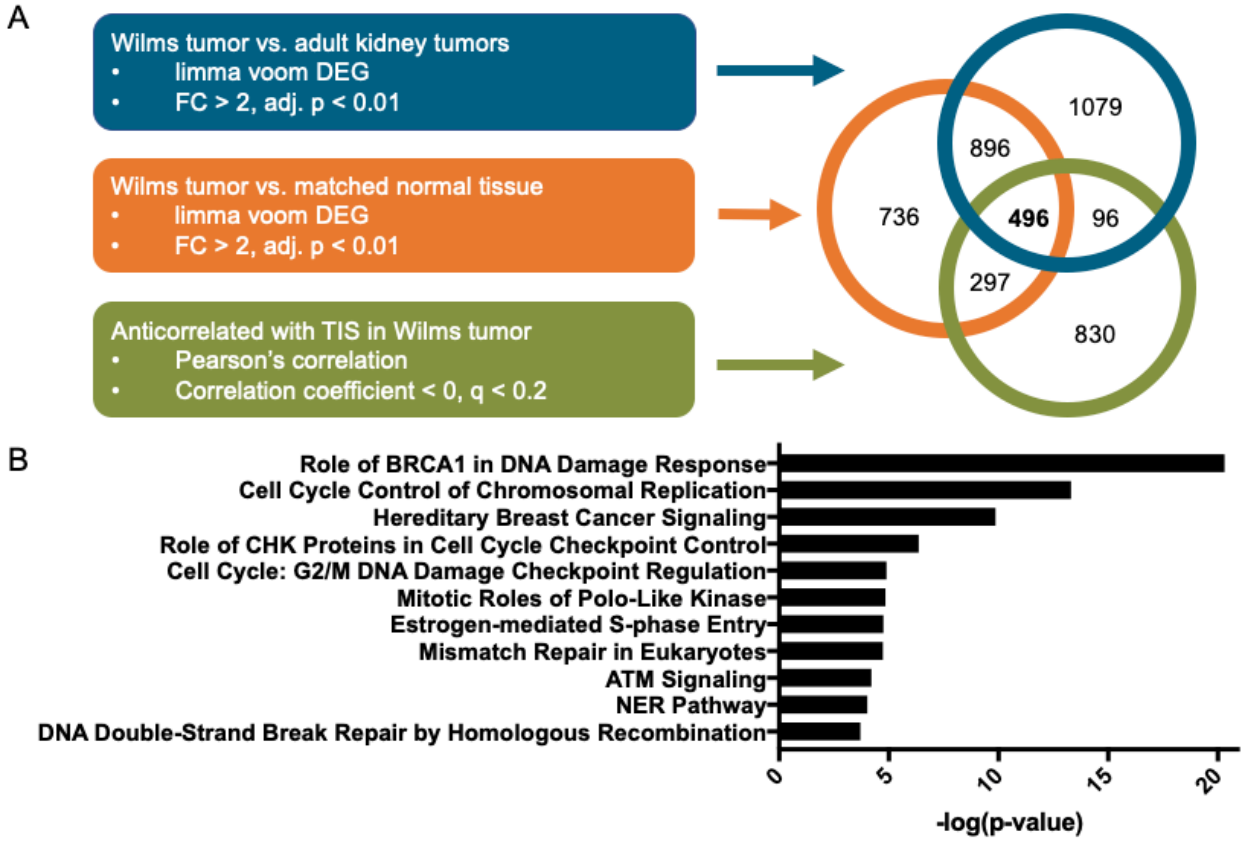

Figure 5.2 Genes upregulated in Wilms tumor and anti-correlated with TIS associate with DNA damage response and repair pathways.
(A) Venn diagram of candidate genes identified by three independent methods. (B) Top pathways identified by Ingenuity Pathway Analysis for 496 candidate genes.

The candidate genes were not limited to one type of DNA repair and instead represented multiple pathways including mismatch repair, nucleotide excision repair, and homologous recombination (Table 5.1). This observation suggests that genes related to the DNA damage response are upregulated and associated with the non-T cell-inflamed phenotype in Wilms

tumor. This set of pathways caught our attention for two reasons. First, loss of DNA repair proteins has been associated not only with carcinogenesis but also with increased generation of mutational neoepitopes[69]. Second, pharmacologic inhibitors of poly (ADP-ribose) polymerase (PARP), which is involved in recognition and repair of single-strand DNA breaks, have been shown to promote anti-tumor immunity through activation of the host STING pathway[70]. Thus, it seemed plausible that increased expression and activation of DNA repair machinery could have the opposite effect and restrain anti-tumor immunity.

DNA Repair Pathway	Upregulated Genes in Wilms
Mismatch Repair	MSH2, MSH6, POLE, EXO1
DNA Damage Checkpoint	BLM, BRCA1, FANCA, MDC1, RAD18, RFC4, RFC5, TOPBP1
Base/Nucleotide Excision Repair	LIG3, PARP1, POLE
Homologous Recombination Repair	BLM, BRCA1, BRCA2, FANCA, FANCG, FANCI, FANCD2
Nonhomologous End-Joining	PRKDC

Table 5.1 DNA repair genes upregulated in Wilms tumors span multiple pathways.
Top DNA repair genes from 496 gene list sorted based on reported literature DNA repair pathway.

To pursue this hypothesis further, we curated a list of DNA repair genes by filtering the 496 genes previously identified by the 480 genes present in the MSigDB GO DNA Repair gene signature. This resulted in a list of 50 genes that were related to DNA repair, upregulated in Wilms tumor, and anti-correlated with TIS in Wilms tumor (Figure 5.3).

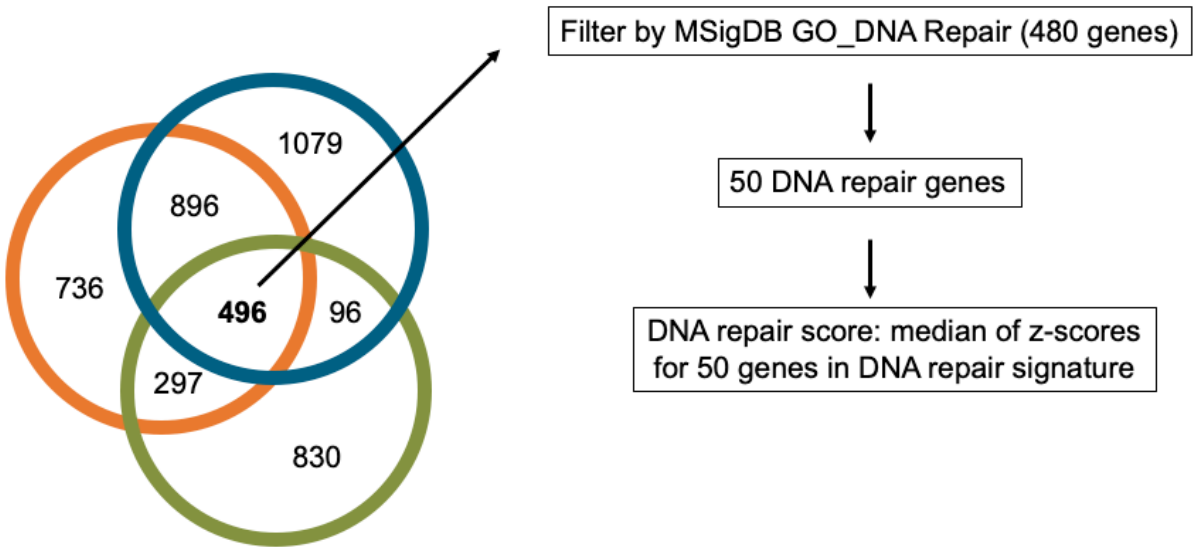

Figure 5.3 Method for developing DNA repair score.
Candidate 496 genes identified from Wilms tumor analysis were filtered by MSigDB GO_DNA Repair signature, which contained 480 genes. This resulted in a filtered list of 50 DNA repair genes from which the DNA repair score was calculated. The DNA repair score was taken as the median of the z-scores for the log2-normalized expression of the 50 genes in the signature.

This 50-gene DNA repair signature was then used to calculate DNA repair expression scores for Wilms tumor as well as other tumor types. Wilms tumor samples had significantly higher DNA repair scores than the other pediatric tumor types tested (Figure 5.4A) and the adult kidney cancer types tested (Figure 5.4B). Additionally, there was a significant negative correlation between TIS and the DNA repair score within Wilms tumor samples (Figure 5.4C). Wilms tumors also had significantly higher DNA repair scores than the matched normal kidney samples (Figure 5.4D), suggesting that high DNA repair activity was not just a property of pediatric kidneys but rather was upregulated in Wilms tumors.

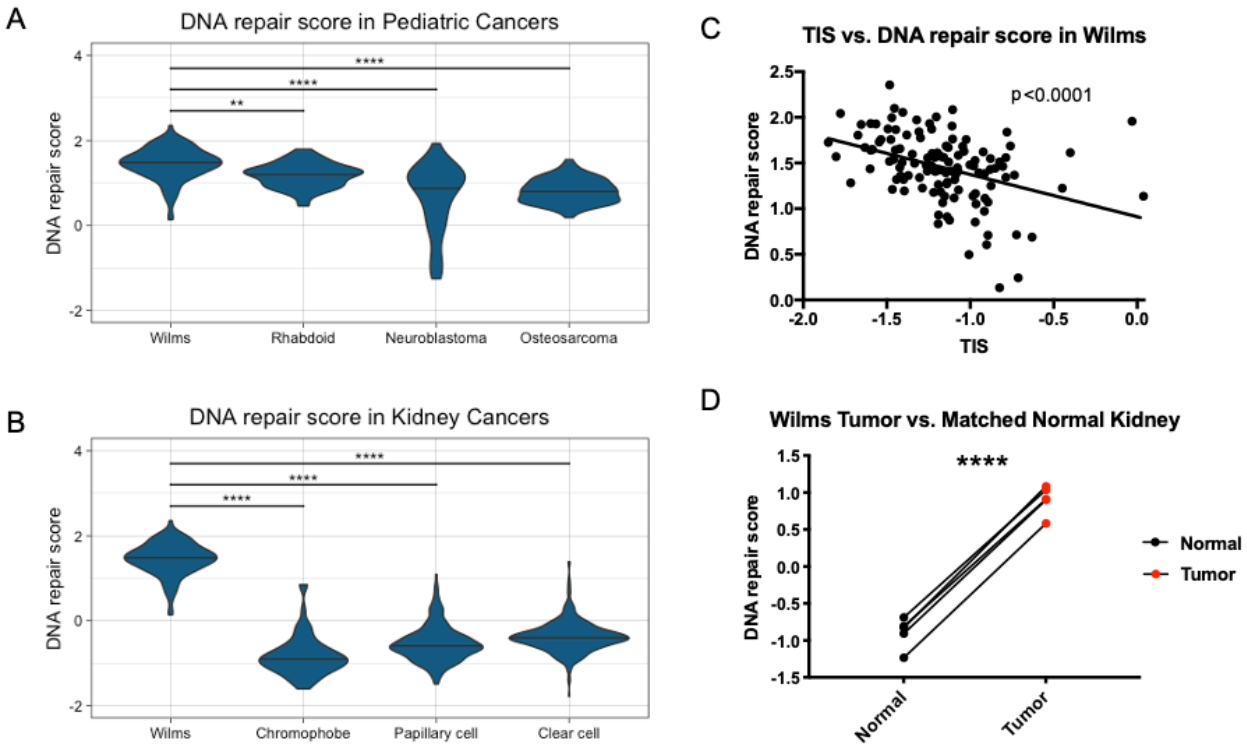

Figure 5.4 Wilms tumors have higher DNA repair scores than other pediatric cancer types, adult kidney cancer types, and matched normal kidney samples.
(A) DNA repair scores in Wilms tumor and the other pediatric tumor types osteosarcoma, neuroblastoma, and rhabdoid tumor. (B) DNA repair scores in Wilms tumor and the other adult kidney tumor types chromophobe, papillary cell, and clear cell renal carcinoma. (C) Correlation between TIS and DNA repair score in Wilms tumor samples. (D) DNA repair scores in Wilms tumor versus matched normal kidney samples.

5.04 DNA repair gene expression negatively correlates with T cell inflammation in adult cancers

The striking negative association between DNA repair score and TIS in Wilms tumor led us to test whether the same could be observed in adult tumor types. Even though overall expression of DNA repair pathway genes was lower in adult tumors, it was still feasible that it negatively correlated with immune cell infiltration. In fact, computing the correlation coefficient between DNA repair score and TIS across the panel of cancers represented in TCGA revealed

that most adult tumor types displayed a negative association between these two gene signatures (Figure 5.5A). Since melanoma samples are relatively more accessible for further study than other tumor types such as Wilms, we looked more specifically within the TCGA metastatic melanoma samples and observed a significant negative correlation between TIS and both the 50-gene DNA repair score (Figure 5.5B) and a score generated from all 480 genes in the MSigDB GO DNA Repair gene signature (Figure 5.5C). This suggested that among other adult tumor types, melanoma displayed the same anti-correlation between DNA repair gene expression and TIS that was seen in Wilms tumor.

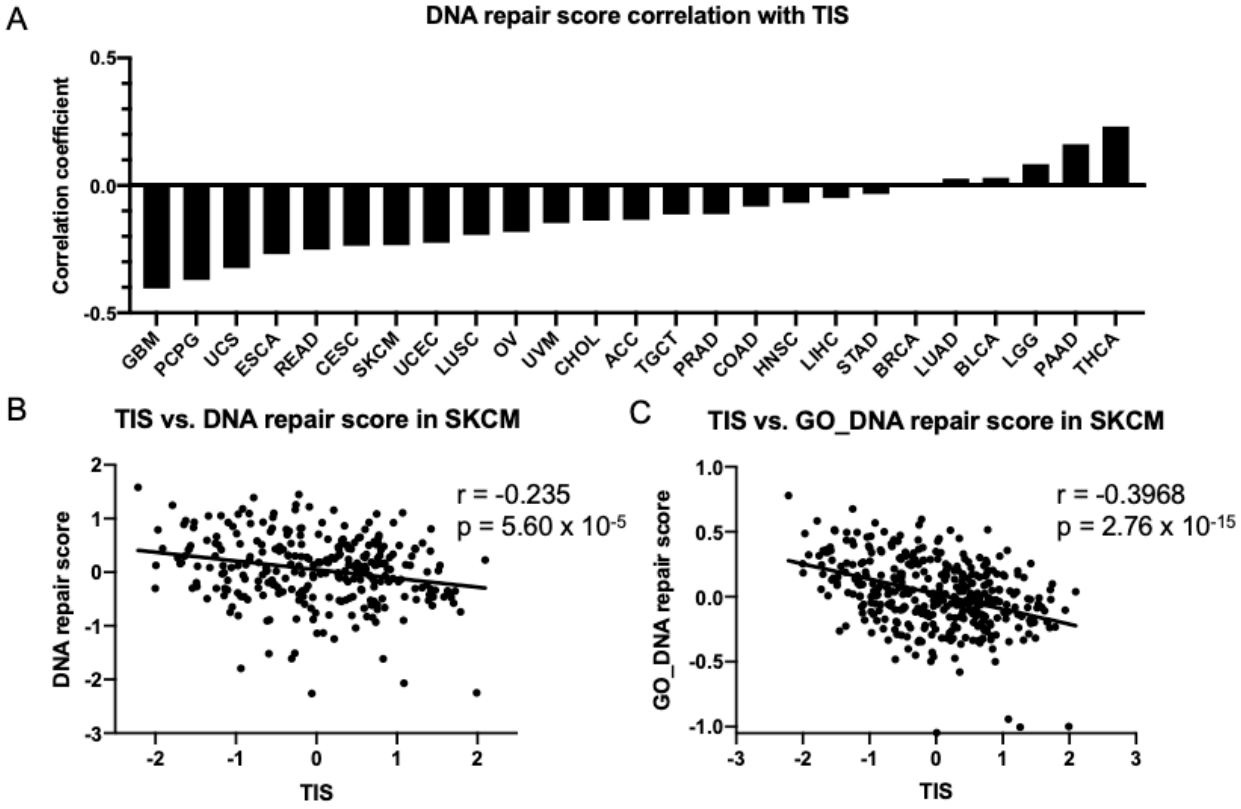

Figure 5.5 TIS significantly anti-correlates with DNA repair score in most TCGA tumor types, including melanoma.
(A) Correlation coefficients for the correlation between TIS and DNA repair score in each TCGA tumor type. (B) Correlation between TIS and DNA repair score in TCGA metastatic melanoma samples. (C) Correlation between TIS and GO_DNA repair gene score in TCGA metastatic melanoma samples.

5.05 DNA repair gene expression associates with T cell inflammation independent of mutation burden

It is well-established that loss of DNA repair genes can rapidly promote the accumulation of mutations in cancer. We next sought to determine if high DNA repair gene expression was associated with a correspondingly low tumor mutation burden, and if that in turn affected T cell inflammation. TCGA data were interrogated for the total number of somatic mutations, and a potential correlation with the DNA repair gene score was sought. Interestingly, in the TCGA melanoma samples, there was not a significant association between DNA repair gene expression and total number of mutations (Figure 5.6A). In addition, the negative association between DNA repair score and TIS in melanoma remained significant after correcting for effects of mutation burden (Figure 5.6B). This was not only true in melanoma, and when mutation effects were regressed out of all TCGA tumors, the majority of tumor types retained a negative correlation between DNA repair score and TIS (Figure 5.6C). These results suggest that the mechanism by which high DNA repair machinery mediates diminished immune cell infiltration is distinct from induction of mutational neoantigens.

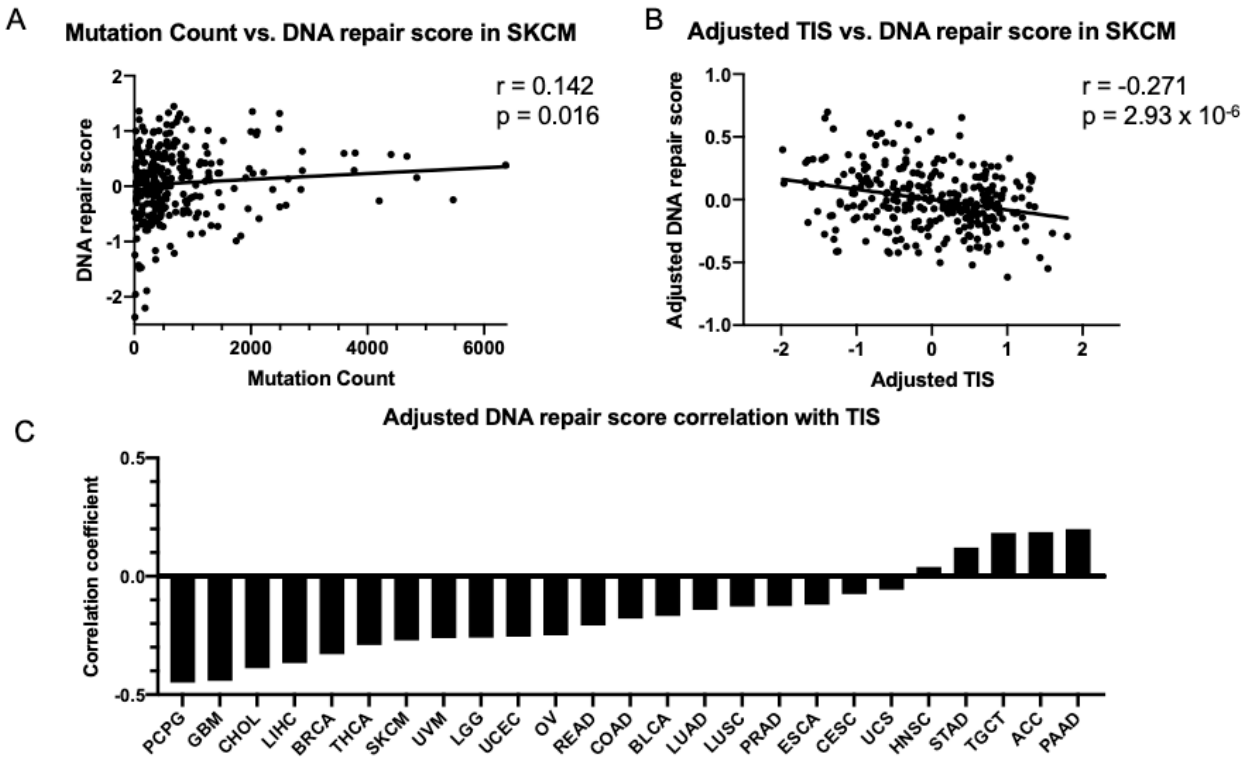

Figure 5.6 TIS does not strongly associate with total mutation count in melanoma and DNA repair score correlation with TIS is not explained by mutation count, Type I IFN score, or proliferation score.
(A) Correlation between DNA repair score and total mutation count in TCGA metastatic melanoma samples. (B) Correlation between TIS and DNA repair score in TCGA metastatic melanoma, adjusted to regress out effect of mutation count. (C) Correlation coefficients for correlation between TIS and DNA repair score in each TCGA tumor type, adjusted to regress out effect of mutation count.

5.06 MSH2$^+$ tumor cells negatively correlate with CD8$^+$ T cells in melanoma and are associated with immunotherapy response

It was desirable to examine a potential correlation between high expression of DNA repair machinery and low immune cell infiltration directly in tumor tissue. MSH2 was one of the top DNA repair genes identified from the Wilms tumor analysis, and MSH2 transcripts were confirmed to have a strong anti-correlation with TIS in melanoma (Figure 5.7). The availability of anti-MSH2 antibodies enabled testing of this hypothesis by immunofluorescence staining,

using a cohort of 30 baseline biopsy samples from metastatic melanoma patients who were treated with anti-PD-1 antibody therapy. Tumor cells were identified by the transcription factor SOX10, and anti-CD8 was used to stain $CD8^+$ T cells.

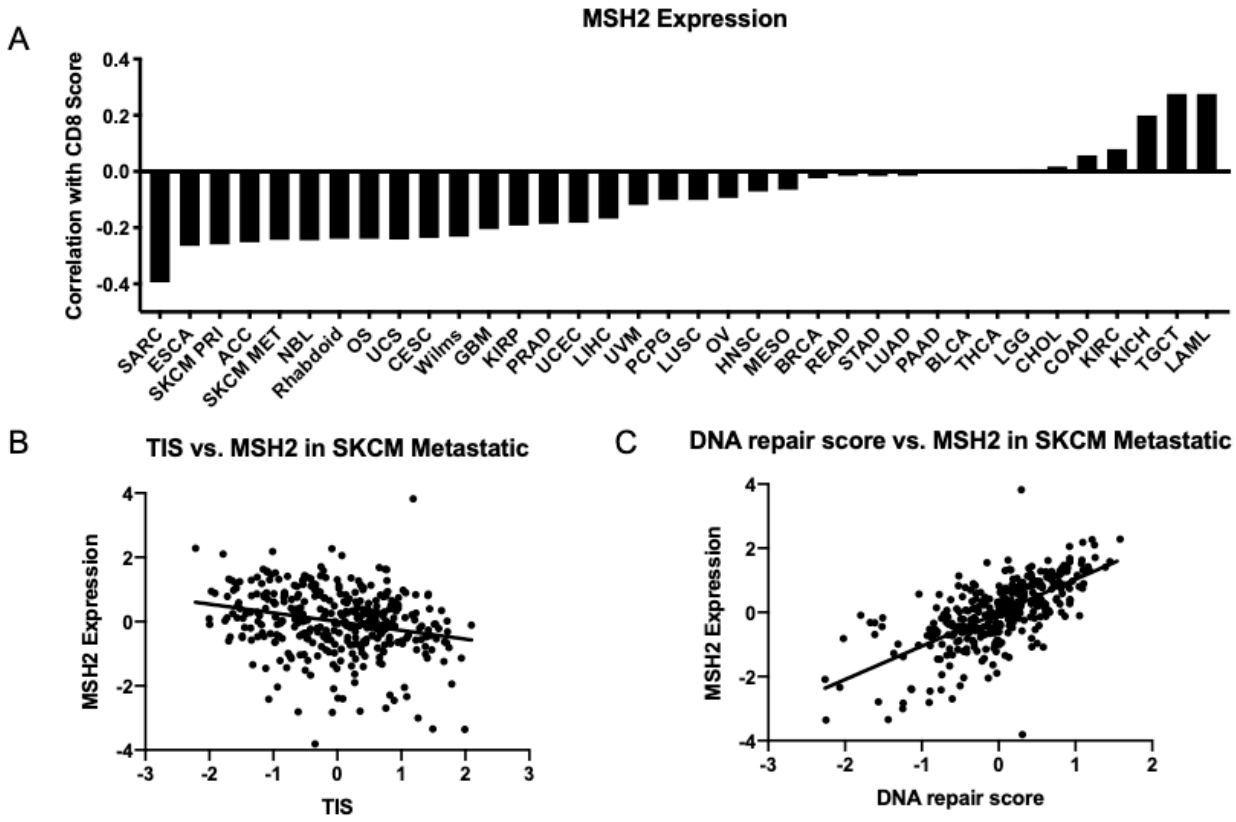

Figure 5.7 MSH2 expression significantly anticorrelates with TIS in most TCGA tumor types, including melanoma.
(A) Correlation coefficients for the correlation between MSH2 expression and TIS in each TCGA tumor type. (B) Correlation between TIS and MSH2 expression in TCGA metastatic melanoma samples. (C) Correlation between DNA repair score and MSH2 expression in TCGA metastatic melanoma samples.

Anti-MSH2 Ab was used in concert, and there was a detectable range of both $MSH2^+$ cells and $CD8^+$ cells in this cohort of samples (Figure 5.8A). Quantifying cell counts from these samples revealed a significant negative correlation between $CD8^+$ T cell numbers and $MSH2^+$

$SOX10^+$ tumor cell numbers (Figure 5.8B). In fact, there were no regions of interest quantified with both above-median numbers of $MSH2^+$ $SOX10^+$ tumor cells and above-median numbers of $CD8^+$ T cells. These data align with the phenotype observed in the RNA sequencing data and suggest that tumors with high numbers of MSH2-expressing tumor cells tend to have reduced $CD8^+$ T cell infiltration.

We then investigated whether high expression of MSH2 by melanoma cells was associated with lack of clinical response to anti-PD-1. Clinical efficacy was categorized into complete response, partial response, stable disease, or progressive disease according to standard RECIST criteria. Interestingly, non-responders to anti-PD-1 immunotherapy had significantly higher numbers of $MSH2^+$ $SOX10^+$ tumor cells than responders (Figure 5.8C), suggesting potential utility of MSH2 staining as a predictive biomarker for lack of response.

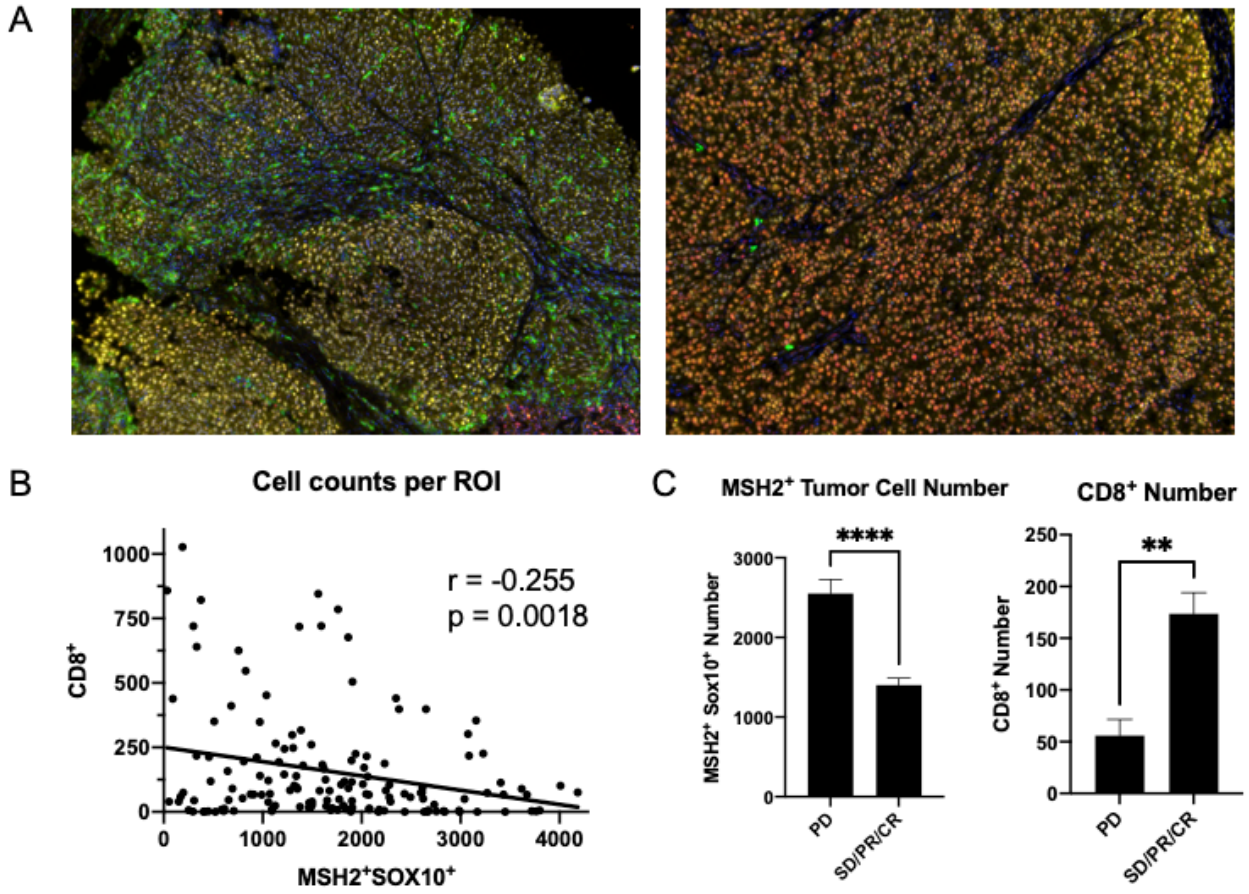

Figure 5.8 MSH2+ tumor cell numbers significantly anti-correlate with CD8+ T cells in melanoma patients and are significantly higher in non-responders to checkpoint blockade immunotherapy.
(A) Example images from immunofluorescent staining of melanoma tissues. MSH2 is shown in red, CD8 is green, SOX10 is yellow, and DAPI is blue. (B) Correlation of $CD8^+$ cells and $MSH2^+SOX10^+$ in each 40X melanoma slide image, 5 images taken per sample. (C) Quantification of $MSH2^+SOX10^+$ and $CD8^+$ cells by ICB response category. Progressive disease = PD, stable disease = SD, partial response = PR, complete response = CR.

5.07 Summary of findings

Among the four pediatric cancers, we observed the lowest T cell inflammation signature (TIS) scores in Wilms tumor. Primary Wilms tumor samples also showed significantly lower TIS scores compared to matched normal tissues, arguing for loss of natural T cell infiltration. Pathway analysis of genes upregulated in Wilms tumor and anti-correlated with TIS revealed

that the most activated pathways involved DNA repair. A parallel analysis was performed in 31 adult cancer types from TCGA, and the majority of adult tumors also showed a high DNA repair score associated with low TIS. Melanoma samples from an independent cohort revealed an inverse correlation between MSH2+ tumor cells and CD8+ T cell numbers. Additionally, melanomas with high MSH2+ tumor cell numbers were largely non-responders to anti-PD-1 therapy. While loss of DNA repair machinery has previously been associated with carcinogenesis and increased mutational antigen generation, our results suggest that hyper-expression of DNA repair genes might be prohibitive for anti-tumor immunity, arguing for pharmacologic targeting of DNA repair as a potential therapeutic strategy.

Chapter 6: Discussion

6.01 STING agonist promise and limitations as a cancer therapeutic

STING agonists demonstrate remarkable activity in murine models, increasing IFN-β production in the tumor microenvironment, promoting tumor-specific T cell priming, and driving near-complete tumor control in transplantable models[22]. Clinical activity of STING agonists in human tumors is an area of active investigation, with many therapeutic candidates currently undergoing evaluation in clinical trials. However, the clinical data reported from early agonists suggests that not all patients respond to these agonists, raising questions regarding mechanism of response versus resistance in individual patients.

The first generation of human STING agonists are cyclic dinucleotides constructed to mimic natural STING agonists but with increased stability and activation of the five major human STING variants[27,28]. These are generally administered via intratumoral injection, which works well if the tumor is easily accessible. However, this route is not well suited for tumors that are not easily injected or for cases in which there are many metastases to treat. This indicates a need to formulate STING agonists that do not require intratumoral injection and can instead be administered systemically.

To this end, several groups have performed chemical compound screens to identify non-nucleotide STING agonists with systemic anti-tumor activity[71–73]. Such compounds can be selected for increased cell permeability and also resistance to hydrolysis by ENPP1[74]. One such screen identified several amidobenzimidazole-based compounds. The investigators linked two of these to create a dimeric ligand with even higher STING binding affinity. This compound demonstrated efficacy in the CT-26 colorectal model when administered IV[75].

Packaging cGAMP in liposomal nanoparticles has demonstrated improved cellular uptake and better tumor control in transplantable and genetically engineered triple negative breast cancer models as well as the B16.F10 melanoma model[76]. Another study found that liposomal formulated STING agonist can cause loss of APC viability, so the authors chose to load a STING agonist ex vivo into exosomes instead (ExoSTING). ExoSTING induced superior IFN-β production compared to soluble STING agonists and the responding mice were protected against tumor re-challenge[77].

Modifying bacteria is an alternative strategy for developing novel STING agonists that can be delivered systemically. The SYN-STING method introduces a di-nucleotide cyclase gene into Escherichia coli Nissle to generate cyclic-di-AMP in the hypoxic tumor microenvironment. SYN-STING demonstrated robust antitumor responses to transplanted tumors and immunologic memory when re-challenged 40+ days after the initial complete response[78]. Another bacterial approach utilizes a highly attenuated strain of salmonella typhimurium that localizes to tumor due to auxotrophic consumption of immunosuppressive adenosine and delivers TREX1 RNAi to block degradation of cytosolic DNA (STACT-TREX1). Following IV delivery, these bacteria were found to be 1000-fold enriched in the tumor compared to liver and spleen and demonstrated CD8-dependent tumor growth inhibition and regression in multiple tumor models[79].

Other novel preclinical strategies activate the STING pathway by targeting regulatory components that indirectly activate STING. For example, ENPP1 inhibitors reduce cGAMP degradation, thus improving STING pathway activation. They can be delivered systemically to increase sensitivity to endogenous STING agonists[80,81]. Blocking endolysosome acidification with bafilomycin A1 (BaFA1) can also support STING signaling by preventing STING degradation. Intratumoral injection of cGAMP and BaFA1 in B16 subcutaneous tumors resulted

in improved tumor control compared to cGAMP alone[82]. As our molecular understanding of the STING pathway and its regulation improves, there will likely be additional opportunities for STING pathway therapeutic targeting beyond administration of cyclic dinucleotides.

It will also be important to better understand the microenvironmental changes induced by type I IFNs elicited by STING pathway activation in both preclinical models and in patients that are responders or non-responders to STING agonists. For example, chronic type I IFN signaling can reportedly have pro-tumor effects including immune suppression and promote metastasis[83]. Most STING agonist studies to date haven't encountered this issue because treatment is performed with one or a few doses that lead to a burst of IFN production that favors immune activation.

The selection of clinical dose is also critical. Single, low dose IT administration of ADU-S100 appears to be optimal for generating tumor-specific T cell responses in mouse models, and this depends on type I IFN signaling. In contrast, high or repetitive doses of ADU-S100 can mediate tumor destruction yet impair the anti-tumor T cell response and memory formation[84]. High doses could be promoting tumor regression through direct cytotoxicity, cytokine-mediated toxicity, or antibody-dependent cell-mediated toxicity or cellular phagocytosis. It is possible that administration of a high IT dose in patients could debulk a primary tumor while providing immunogenic doses of STING agonist systemically. Alternatively, lower doses may prove more efficacious due to their advantage in generating an adaptive immune response.

A greater mechanistic understanding of the STING pathway may allow for the development of agents to more potently activate it and to selectively induce desired outputs while avoiding immune-suppressive effects. For example, STING pathway activation is linked to multiple inhibitory feedback loops including AIM2 inflammasome activation, autophagy

induction, and autocrine IFN signaling which are all thought to help attenuate STING signaling[85]. Agents designed to disrupt one or more of these feedback loops might synergistically interact with STING agonists or act as single agents. These compounds would not directly activate the pathway but rather would serve to increase the sensitivity or magnitude of signaling output of STING signaling activated by endogenous tumors. In this way, these agents may work well as systemic therapies, only increasing sensitivity of the pathway and therefore perhaps only eliciting activation at tumor sites.

6.02 Synergy between innate pathways improves IFN-β production and tumor control

While ongoing clinical studies continue to optimize the dose, schedule, and formulation of therapeutic STING agonists, there may also be opportunity for mechanistic studies to identify ways of improving anti-tumor immune responses in the context of STING agonists. In chapter three we describe the observation initially made in macrophages that stimulation with LPS + the STING agonist DMXAA induces more IFN-β transcription than either agonist is capable of inducing alone. Mechanistically, this seems to be due to differential transcription factor activation downstream of each pathway (IRF3 downstream of STING and NFκB downstream of TLR4), and these transcription factors working together to optimally promote IFN-β production.

IRF3 activation downstream of STING has been well-characterized, and most studies of STING signaling have focused on this arm of the pathway[17,86,87]. More recently however, there has been some evidence implicating a role for NFκB as well[88]. Three distant "Alu" sites associate with the IFN-β locus and are bound by NFκB prior to it binding the IFN-β promotor[89]. While further characterization is needed, it is thought that NFκB binding to these "Alu" sites

may epigenetically open the IFN-β promotor region and allow the other transcription factors to bind. Our results indicate that NFκB activation downstream of STING agonist treatment is significantly less than NFκB activation downstream of LPS treatment. This could help explain why LPS is able to dramatically augment IFN-β transcription, if NFκB is required for optimal IFN-β locus accessibility.

Another important consideration is that not every cell produces IFN-β following stimulation, and that proper transcription factor binding leading to transcription is a stochastic process. Evidence for this comes from the fact that single cell cloning from a pool of cells capable of expressing IFN-β produces pools of cells that express IFN-β at the same proportion[90]. This could be due to the fact that there is a limited supply of the transcription factors binding to IFN-β, and that there may not be sufficient quantities of each free to bind the IFN-β in every cell. Consistent with this hypothesis, overexpression of either IRF3 or NFκB results in a higher proportion of cells that express IFN-β[91,92]. This raises an interesting question as to whether LPS stimulation drives more IFN-β production per cell or whether it increases the number of cells that produce IFN-β.

Additionally, LPS promoted tumor control in vivo when combined with low dose STING agonist administration. The ability to achieve a robust anti-tumor immune response with lower STING agonist doses may protect against some of the negative effects of STING agonist therapy. Treatment with high-dose STING agonist has been shown to actually result in reduced tumor-specific T cell priming and can even be cytotoxic to T cells, as T cell intrinsic STING signaling can promote apoptosis.

6.03 Flt3L can overcome the CD103$^+$ DC defect in BPC tumors

As tumors develop in the context of an intact immune system, they become shaped by immunological pressure from the environment in which they establish. This process is dynamic, and cancers have been shown to evolve in ways that allow them to escape T cell recognition. Examples of this include loss of β_2-microglobulin (B2M) and HLA gene expression emerging in tumors that initially responded to checkpoint blockade or adoptive T cell-based therapies but went on to acquire resistance and progress[93–95]. Since B2M is required for surface expression of peptides on MHCI, loss of B2M allows tumors to evade recognition by T cells. Mutations in genes such as B2M and HLA have been demonstrated in a range of tumor types, and likely arose in response to immunological pressure[96–98].

Evolving in such a way that blocks T cell accumulation in the first place may also convey a survival advantage to tumors. Case studies in metastatic melanoma have identified tumors that initially responded to peptide vaccine or checkpoint blockade therapy, then developed treatment-resistant metastases with aberrant β-catenin activation or acquired PTEN loss[99]. In both cases, these alterations were associated with loss of T cell infiltration. This suggests it is advantageous for tumors to manipulate these pathways and resist T cell entry. Accordingly, WNT/β-catenin pathway activation is widely observed in non-T cell-inflamed tumors across many tumor types.

Identifying ways to overcome such pathways that prevent immune infiltration will be critical to achieving therapeutic benefit in these patients. In the case of β-catenin, the defect appears to be upstream of T cell recruitment, as BPC mouse tumors lack CD103$^+$ DC infiltration and display poor expression of the chemokines known to recruit them[38]. Intratumoral injection of in vitro-activated, bone marrow derived DCs did promote tumor control in this model and improve the response to anti-PD-L1 + anti-CTLA-4 therapy. This indicates that DCs in the tumor

microenvironment are sufficient to overcome the non-T cell-inflamed BPC model, however this approach would be costly and hard to scale in human patients.

This led us to test if we could induce DC accumulation by another method. We chose to evaluate intratumoral injection of Flt3L, which has been previously shown to be capable of expanding $CD103^+$ DC progenitors[100]. We observed that one dose of Flt3L followed by one dose of the STING agonist DMXAA was able to sensitize BPC tumors to anti-PD-L1 + anti-CTLA-4 therapy. Neither Flt3L nor DMXAA was able to do this alone, indicating that these DCs must be activated in order to generate a productive anti-tumor T cell response.

6.04 DNA damage triggers innate immune activation

Compared to adult tumor types, relatively little is known about the immune landscape of pediatric tumors and their associated mechanisms of immune resistance. Using RNA sequencing data, we showed that Wilms tumors demonstrate significantly lower T cell inflammation signatures than matched normal kidney samples, other pediatric tumor samples, and other adult kidney tumor samples. Pathway analysis identified multiple types of DNA repair are upregulated in Wilms tumor and anti-correlated with TIS scores.

Rapidly proliferating cells in the tumor microenvironment experience high levels of replicative and oxidative stress that can lead to DNA damage[101]. Disruption of specific DNA polymerases as well as repair enzymes such as BLM, BRCA2, and RNAseH2 promote genome instability and the formation of micronuclei, which can then be detected by the enzyme cGAS to trigger an innate immune response[20-24]. For example, polymerase ζ-deficient cells accumulated micronuclei and induced expression of interferon-stimulated genes in a cGAS- and STING-dependent manner[102]. In response to acute BRCA2 abrogation, tumor cells accumulated

micronuclei and limited proliferation by G1 cell cycle arrest. As the cells adapted to chronic BRCA2 loss, they re-entered the cell cycle with a concomitant upregulation of interferon-stimulated genes that was dependent on STING and STAT1[103]. Additionally, the upregulation of interferon genes following loss of EXO1 or BLM could be reversed by knocking out TREX1, an enzyme that degrades cytosolic DNA[104]. Taken together these data support the notion that DNA repair disruption can trigger innate immune activation through induction of interferon signaling following micronuclei sensing.

6.05 Overexpression of DNA repair genes may limit immune activation

Our observations in Wilms tumor suggest the converse may also be true, and that increased tumor expression of DNA repair genes is associated with a less robust immune response, potentially due to reduced cGAS-STING pathway activation. Previous work from our lab and others showed that type I interferon signaling is correlated with activated T cell gene signatures in human tumors and required for tumor-specific T cell priming in mice[105]. By creating a DNA repair score from the DNA repair genes identified in Wilms tumor, we were able to test whether DNA repair gene expression is negatively associated with T cell inflammation in adult tumor types as well. It is known that high levels of tumor microsatellite instability are associated in adult tumors with increased lymphocyte infiltration, reduced metastasis, and improved survival as well as response to checkpoint blockade immunotherapy[106–108].

Alternatively, some tumors have been shown to upregulate DNA repair genes, such as MGMT, RRM2, POLE2, and TTK, which associated with increased invasiveness and metastasis, poor outcomes, and resistance to therapy[109–113]. These observations led to the hypothesis that overexpression of MMR genes could improve cellular resistance to DNA lesions as well as

survival following DNA damage[114]. We believe this could also promote tumor immune evasion, as we identified a significant negative correlation between DNA repair and activated T cell signatures in the majority of TCGA tumor types. This suggests a reduced endogenous anti-tumor immune response when DNA repair gene expression is high. If this is the case, reversing the phenotype with DNA repair inhibitors may be a viable strategy to sensitize tumors to immune checkpoint blockade therapy. This concept is supported by our finding that responders to anti-PD-1 blocking antibodies have significantly fewer $MSH2^+$ tumor cells.

Surprisingly, we did not observe a strong association between the DNA repair gene expression score and total mutation number in melanoma, and the negative relationship between DNA repair score and TIS remained strong across TCGA when correcting for mutation count. This indicates a potential role for DNA repair genes outside of preventing the accumulation of mutations and warrants further investigation. In summary, we found that independent of mutation count, high DNA repair gene expression is linked to low immune activation across tumor types and linked to T cell infiltration and immunotherapy response in melanoma. Upregulating the expression of DNA repair genes may be a mechanism by which tumors evade immune destruction, which could explain the increased aggressiveness and therapy resistance observed in tumors overexpressing these factors.

6.06 Conclusions

STING and other innate immune agonists have shown clinical promise and are an exciting strategy to generate anti-tumor immune responses when the endogenous response is poor. However, the fact that many patients do not respond to these agonists highlights the need to better understand mechanisms of response versus resistance in order to improve clinical

outcomes. In this study, we take three separate approaches to interrogate potential determinants of resistance to STING agonist therapy.

First, we examined the hypothesis that in these cases activating the STING pathway alone is insufficient to optimally induce IFN-β transcription, and that using a combination of innate immune agonists is superior. We found that a combination of the STING agonist DMXAA and LPS had a synergistic effect on IFN-β transcription in vitro, which was due to improved NFκB activation downstream of LPS. This combination also improved in vivo tumor control and may represent a viable therapeutic strategy to improve STING agonist response rates and mitigate some of the negative effects associated with higher doses of STING agonist therapy.

Next, we explored the possibility that STING agonists may not be effective in tumors which lack the $CD103^+$ DC subset required for optimal tumor-specific T cell priming. To test this, we used the BPC genetic mouse model of melanoma, which has been previously shown to lack robust infiltration of $CD103^+$ DCs and $CD8^+$ T cells and is refractory to anti-PD-L1 + anti-CTLA-4 checkpoint blockade therapy. The STING agonist DMXAA is also ineffective at promoting tumor control in these mice and does not sensitize them to checkpoint blockade antibodies. We believe this to be due to the fact that DMXAA increases $CD8^+$ T cell infiltration in this model but not infiltration of $CD103^+$ DCs. Interestingly, Flt3L can overcome the deficiency of $CD103^+$ DCs in BPC mice, and when Flt3L is administered in combination with DMXAA, these tumors become sensitive to anti-PD-L1 + anti-CTLA-4. This novel approach utilizes what is known about the requirements for a successful endogenous anti-tumor immune response to overcome the upstream defect driving this non-inflamed phenotype. Future studies will evaluate the potential for clinical use of this combination.

Finally, we examine non-T cell-inflamed human tumors from a tumor-intrinsic perspective to identify new mechanisms that could lead to this phenotype by blocking immune infiltration into tumors. To do this, we focused on the relatively non-inflamed Wilms tumor and probed transcriptional data from human tumor samples. We identified differentially expressed genes in Wilms tumors compared to other pediatric tumor types, adult kidney tumor types, and genes that anti-correlated with T cell inflammation signature within Wilms tumors. Pathway analysis of these genes revealed high expression of DNA repair factors in non-T cell-inflamed Wilms tumors. This observation was also seen across several adult tumors in TCGA, and in metastatic melanoma samples stained for CD8, MSH2, and SOX10, there was a negative association between $CD8^+$ (T cell) numbers and $MSH2^+$ $SOX10^+$ (MSH2-expressing tumor cell) numbers. This suggests that high levels of the DNA repair protein MSH2 are anti-correlated with T cells in these samples, and we also found that patients with high $MSH2^+$ $SOX10^+$ tumor cell counts tended to be non-responders to anti-PD-1 therapy. Loss of DNA repair factors has been associated with increased tumor immunogenicity, but to our knowledge this is the first implication of high DNA repair levels with the non-T cell-inflamed phenotype.

Ultimately, these three approaches have yielded novel insights for understanding and overcoming the non-T cell-inflamed tumor microenvironment by identifying a novel way in which tumors may exclude immune cells, a way of accumulating the critical immune subsets when they are absent, and a way of activating them more optimally when they are recruited to the tumor microenvironment.

References

1. Shankaran, V. *et al.* IFNγ and lymphocytes prevent primary tumour development and shape tumour immunogenicity. *Nature* **410**, 1107–1111 (2001).
2. Hanahan, D. & Weinberg, R. A. Hallmarks of Cancer: The Next Generation. *Cell* **144**, 646–674 (2011).
3. Mantovani, A., Romero, P., Palucka, A. K. & Marincola, F. M. Tumour immunity: effector response to tumour and role of the microenvironment. *The Lancet* **371**, 771–783 (2008).
4. Dunn, G. P., Old, L. J. & Schreiber, R. D. The Three Es of Cancer Immunoediting. *Annu. Rev. Immunol.* **22**, 329–360 (2004).
5. Dunn, G. P., Koebel, C. M. & Schreiber, R. D. Interferons, immunity and cancer immunoediting. *Nat. Rev. Immunol.* **6**, 836–848 (2006).
6. Freeman, G. J. *et al.* Engagement of the Pd-1 Immunoinhibitory Receptor by a Novel B7 Family Member Leads to Negative Regulation of Lymphocyte Activation. *J. Exp. Med.* **192**, 1027–1034 (2000).
7. Vaddepally, R. K., Kharel, P., Pandey, R., Garje, R. & Chandra, A. B. Review of Indications of FDA-Approved Immune Checkpoint Inhibitors per NCCN Guidelines with the Level of Evidence. *Cancers* **12**, (2020).
8. Ayers, M. *et al.* IFN-γ–related mRNA profile predicts clinical response to PD-1 blockade. *J. Clin. Invest.* **127**, 2930–2940 (2017).
9. Tumeh, P. C. *et al.* PD-1 blockade induces responses by inhibiting adaptive immune resistance. *Nature* **515**, 568–571 (2014).
10. Trujillo, J. A., Sweis, R. F., Bao, R. & Luke, J. J. T Cell–Inflamed versus Non-T Cell–Inflamed Tumors: A Conceptual Framework for Cancer Immunotherapy Drug

Development and Combination Therapy Selection. *Cancer Immunol. Res.* **6**, 990–1000 (2018).

11. Mikucki, M. E. *et al.* Non-redundant requirement for CXCR3 signalling during tumoricidal T-cell trafficking across tumour vascular checkpoints. *Nat. Commun.* **6**, ncomms8458 (2015).
12. Mikucki, M. E. *et al.* Unlocking tumor vascular barriers with CXCR3: Implications for cancer immunotherapy. *OncoImmunology* **5**, e1116675 (2016).
13. Woo, S.-R. *et al.* STING-Dependent Cytosolic DNA Sensing Mediates Innate Immune Recognition of Immunogenic Tumors. *Immunity* **41**, 830–842 (2014).
14. Sun, L., Wu, J., Du, F., Chen, X. & Chen, Z. J. Cyclic GMP-AMP Synthase Is a Cytosolic DNA Sensor That Activates the Type I Interferon Pathway. *Science* **339**, 786–791 (2013).
15. Ogawa, E., Mukai, K., Saito, K., Arai, H. & Taguchi, T. The binding of TBK1 to STING requires exocytic membrane traffic from the ER. *Biochem. Biophys. Res. Commun.* (2018) doi:10.1016/j.bbrc.2018.05.199.
16. Liu, S. *et al.* Phosphorylation of innate immune adaptor proteins MAVS, STING, and TRIF induces IRF3 activation. *Science* **347**, aaa2630 (2015).
17. Ishikawa, H., Ma, Z. & Barber, G. N. STING regulates intracellular DNA-mediated, type I interferon-dependent innate immunity. *Nature* **461**, 788–792 (2009).
18. Fu, J. *et al.* STING agonist formulated cancer vaccines can cure established tumors resistant to PD-1 blockade. *Sci. Transl. Med.* **7**, 283ra52-283ra52 (2015).
19. Hildner, K. *et al.* Batf3 Deficiency Reveals a Critical Role for CD8α+ Dendritic Cells in Cytotoxic T Cell Immunity. *Science* **322**, 1097–1100 (2008).

20. Spranger, S., Dai, D., Horton, B. & Gajewski, T. F. Tumor-Residing Batf3 Dendritic Cells Are Required for Effector T Cell Trafficking and Adoptive T Cell Therapy. *Cancer Cell* **31**, 711-723.e4 (2017).

21. Fuertes, M. B. *et al.* Host type I IFN signals are required for antitumor CD8+ T cell responses through CD8α+ dendritic cells. *J. Exp. Med.* **208**, 2005–2016 (2011).

22. Corrales, L. *et al.* Direct Activation of STING in the Tumor Microenvironment Leads to Potent and Systemic Tumor Regression and Immunity. *Cell Rep.* **11**, 1018–1030 (2015).

23. Baguley, B. C. & Ching, L.-M. DMXAA: An antivascular agent with multiple host responses. *Int. J. Radiat. Oncol.* **54**, 1503–1511 (2002).

24. Baguley, B. C. Antivascular therapy of cancer: DMXAA. *Lancet Oncol.* **4**, 141–148 (2003).

25. Jassar, A. S. *et al.* Activation of Tumor-Associated Macrophages by the Vascular Disrupting Agent 5,6-Dimethylxanthenone-4-Acetic Acid Induces an Effective CD8+ T-Cell–Mediated Antitumor Immune Response in Murine Models of Lung Cancer and Mesothelioma. *Cancer Res.* **65**, 11752–11761 (2005).

26. Prantner, D. *et al.* 5,6-Dimethylxanthenone-4-acetic acid (DMXAA) activates stimulator of interferon gene (STING)-dependent innate immune pathways and is regulated by mitochondrial membrane potential. *J. Biol. Chem.* **287**, 39776–39788 (2012).

27. Meric-Bernstam, F. *et al.* Phase Ib study of MIW815 (ADU-S100) in combination with spartalizumab (PDR001) in patients (pts) with advanced/metastatic solid tumors or lymphomas. *J. Clin. Oncol.* **37**, 2507–2507 (2019).

28. Harrington, K. J. *et al.* Preliminary results of the first-in-human (FIH) study of MK-1454, an agonist of stimulator of interferon genes (STING), as monotherapy or in combination

with pembrolizumab (pembro) in patients with advanced solid tumors or lymphomas. *Ann. Oncol.* **29**, viii712 (2018).

29. O'Neill, L. A. J., Golenbock, D. & Bowie, A. G. The history of Toll-like receptors — redefining innate immunity. *Nat. Rev. Immunol.* **13**, 453–460 (2013).
30. Cui, J., Chen, Y., Wang, H. Y. & Wang, R.-F. Mechanisms and pathways of innate immune activation and regulation in health and cancer. *Hum. Vaccines Immunother.* **10**, 3270–3285 (2014).
31. Thanos, D. & Maniatis, T. Virus induction of human IFNβ gene expression requires the assembly of an enhanceosome. *Cell* **83**, 1091–1100 (1995).
32. Panne, D. The enhanceosome. *Curr. Opin. Struct. Biol.* **18**, 236–242 (2008).
33. Coley, W. B. The Treatment of Malignant Tumors by Repeated Inoculations of Erysipelas: With a Report of Ten Original Cases.1: Bibliography. *Am. J. Med. Sci. 1827-1924* **105**, 487 (1893).
34. SENN, N. THE TREATMENT OF MALIGNANT TUMORS BY THE TOXINS OF THE STREPTOCOCCUS OF ERYSIPELAS. *J. Am. Med. Assoc.* **XXV**, 131–134 (1895).
35. McCarthy, E. F. The Toxins of William B. Coley and the Treatment of Bone and Soft-Tissue Sarcomas. *Iowa Orthop. J.* **26**, 154–158 (2006).
36. Hanna, E., Abadi, R. & Abbas, O. Imiquimod in dermatology: an overview. *Int. J. Dermatol.* **55**, 831–844 (2016).
37. Smith, M. *et al.* Trial Watch: Toll-like receptor agonists in cancer immunotherapy. *OncoImmunology* **7**, e1526250 (2018).
38. Spranger, S., Bao, R. & Gajewski, T. F. Melanoma-intrinsic β-catenin signalling prevents anti-tumour immunity. *Nature* **523**, 231–235 (2015).

39. Tiberio, L. *et al.* Chemokine and chemotactic signals in dendritic cell migration. *Cell. Mol. Immunol.* **15**, 346–352 (2018).

40. Danaher, P. *et al.* Pan-cancer adaptive immune resistance as defined by the Tumor Inflammation Signature (TIS): results from The Cancer Genome Atlas (TCGA). *J. Immunother. Cancer* **6**, 63 (2018).

41. Sweis, R. F. *et al.* Molecular Drivers of the Non–T-cell-Inflamed Tumor Microenvironment in Urothelial Bladder Cancer. *Cancer Immunol. Res.* **4**, 563–568 (2016).

42. Luke, J. J., Bao, R., Sweis, R. F., Spranger, S. & Gajewski, T. F. WNT/β-catenin Pathway Activation Correlates with Immune Exclusion across Human Cancers. *Clin. Cancer Res.* **25**, 3074–3083 (2019).

43. Peng, W. *et al.* Loss of PTEN Promotes Resistance to T Cell–Mediated Immunotherapy. *Cancer Discov.* **6**, 202–216 (2016).

44. Shrimali, R. K. *et al.* Antiangiogenic Agents Can Increase Lymphocyte Infiltration into Tumor and Enhance the Effectiveness of Adoptive Immunotherapy of Cancer. *Cancer Res.* **70**, 6171–6180 (2010).

45. Knight, D. A. *et al.* Host immunity contributes to the anti-melanoma activity of BRAF inhibitors. *J. Clin. Invest.* **123**, 1371–1381 (2013).

46. Ichimura, K. Molecular pathogenesis of IDH mutations in gliomas. *Brain Tumor Pathol.* **29**, 131–139 (2012).

47. Kohanbash, G. *et al.* Isocitrate dehydrogenase mutations suppress STAT1 and $CD8^+$ T cell accumulation in gliomas. *J. Clin. Invest.* **127**, 1425–1437 (2017).

48. Dang, L. *et al.* Cancer-associated IDH1 mutations produce 2-hydroxyglutarate. *Nature* **462**, 739–744 (2009).

49. Sonn, G. & Shortliffe, L. M. Management of Wilms tumor: current standard of care. *Nat. Clin. Pract. Urol.* **5**, 551–560 (2008).

50. Szychot, E., Apps, J. & Pritchard-Jones, K. Wilms' tumour: biology, diagnosis and treatment. *Transl. Pediatr.* **3**, 124–124 (2014).

51. Stahl, D. *et al.* Prognostic Gene Expression, Stemness and Immune Microenvironment in Pediatric Tumors. *Cancers* **13**, 854 (2021).

52. Gadd, S. *et al.* A Children's Oncology Group and TARGET initiative exploring the genetic landscape of Wilms tumor. *Nat. Genet.* **49**, 1487–1494 (2017).

53. Schmitt, J. *et al.* Autoantibody Signature Differentiates Wilms Tumor Patients from Neuroblastoma Patients. *PLOS ONE* **6**, e28951 (2011).

54. Danaher, P. *et al.* Gene expression markers of Tumor Infiltrating Leukocytes. *J. Immunother. Cancer* **5**, 18 (2017).

55. Li, C.-M. *et al.* CTNNB1 Mutations and Overexpression of Wnt/β-Catenin Target Genes in WT1-Mutant Wilms' Tumors. *Am. J. Pathol.* **165**, 1943–1953 (2004).

56. Tian, F., Yourek, G., Shi, X. & Yang, Y. The development of Wilms tumor: From WT1 and microRNA to animal models. *Biochim. Biophys. Acta BBA - Rev. Cancer* **1846**, 180–187 (2014).

57. Luke, J. J., Bao, R., Sweis, R. F., Spranger, S. & Gajewski, T. F. WNT/β-catenin pathway activation correlates with immune exclusion across human cancers. *Clin. Cancer Res.* clincanres.1942.2018 (2019) doi:10.1158/1078-0432.CCR-18-1942.

58. Holl, E. K. *et al.* Immune expression in children with Wilms tumor: a pilot study. *J. Pediatr. Urol.* **15**, 441.e1-441.e8 (2019).

59. Fiore, P. F. *et al.* Wilms' Tumor Primary Cells Display Potent Immunoregulatory Properties on NK Cells and Macrophages. *Cancers* **13**, 224 (2021).

60. Cantoni, C. *et al.* Stromal-like Wilms tumor cells induce human Natural Killer cell degranulation and display immunomodulatory properties towards NK cells. *Oncoimmunology* **10**,.

61. Routh, J. C. *et al.* B7-H1 Expression in Wilms Tumor: Correlation With Tumor Biology and Disease Recurrence. *J. Urol.* **179**, 1954–1960 (2008).

62. Routh, J. C., Grundy, P. E., Anderson, J. R., Retik, A. B. & Kurek, K. C. B7-H1 as a Biomarker for Therapy Failure in Patients with Favorable Histology Wilms Tumor. *J. Urol.* **189**, 1487–1492 (2013).

63. Mardanpour, K., Rahbar, M., Mardanpour, S., Mardanpour, N. & Rezaei, M. CD8+ T-cell lymphocytes infiltration predict clinical outcomes in Wilms' tumor. *Tumor Biol.* **42**, 1010428320975976 (2020).

64. Roberson, S. M. & Walker, W. S. Immortalization of cloned mouse splenic macrophages with a retrovirus containing the v-raf/mil and v-myc oncogenes. *Cell. Immunol.* **116**, 341–351 (1988).

65. Blank, C. *et al.* PD-L1/B7H-1 Inhibits the Effector Phase of Tumor Rejection by T Cell Receptor (TCR) Transgenic CD8+ T Cells. *Cancer Res.* **64**, 1140–1145 (2004).

66. Benjamini, Y. & Hochberg, Y. Controlling the False Discovery Rate: A Practical and Powerful Approach to Multiple Testing. *J. R. Stat. Soc. Ser. B Methodol.* **57**, 289–300 (1995).

67. Cueto, F. J. & Sancho, D. The Flt3L/Flt3 Axis in Dendritic Cell Biology and Cancer Immunotherapy. *Cancers* **13**, 1525 (2021).

68. Young, M. D. *et al.* Single-cell transcriptomes from human kidneys reveal the cellular identity of renal tumors. *Science* **361**, 594–599 (2018).

69. Ciombor, K. K. & Goldberg, R. M. Hypermutated Tumors and Immune Checkpoint Inhibition. *Drugs* **78**, 155–162 (2018).

70. Gupta, P. D. *et al.* PARP and PI3K inhibitor combination therapy eradicates c-MYC-driven murine prostate cancers via cGAS/STING pathway activation within tumor-associated macrophages. *bioRxiv* 2020.07.17.198598 (2020) doi:10.1101/2020.07.17.198598.

71. Chin, E. N. *et al.* Antitumor activity of a systemic STING-activating non-nucleotide cGAMP mimetic. *Science* **369**, 993–999 (2020).

72. Pan, B.-S. *et al.* An orally available non-nucleotide STING agonist with antitumor activity. *Science* **369**, (2020).

73. Berger, G. & Lawler, S. E. Novel non-nucleotidic STING agonists for cancer immunotherapy. *Future Med. Chem.* **10**, 2767–2769 (2018).

74. Li, L. *et al.* Hydrolysis of 2′3′-cGAMP by ENPP1 and design of nonhydrolyzable analogs. *Nat. Chem. Biol.* **10**, 1043–1048 (2014).

75. Ramanjulu, J. M. *et al.* Design of amidobenzimidazole STING receptor agonists with systemic activity. *Nature* **564**, 439 (2018).

76. Cheng, N. *et al.* A nanoparticle-incorporated STING activator enhances antitumor immunity in PD-L1–insensitive models of triple-negative breast cancer. *JCI Insight* **3**, (2018).

77. Jang, S. C. *et al.* ExoSTING, an extracellular vesicle loaded with STING agonists, promotes tumor immune surveillance. *Commun. Biol.* **4**, 1–17 (2021).

78. Leventhal, D. S. *et al.* Immunotherapy with engineered bacteria by targeting the STING pathway for anti-tumor immunity. *Nat. Commun.* **11**, 2739 (2020).

79. Makarova, A. M. *et al.* Abstract 5016: STACT-TREX1: A systemically-administered STING pathway agonist targets tumor-resident myeloid cells and induces adaptive anti-tumor immunity in multiple preclinical models. *Cancer Res.* **79**, 5016–5016 (2019).

80. Carozza, J. A. *et al.* Structure-Aided Development of Small-Molecule Inhibitors of ENPP1, the Extracellular Phosphodiesterase of the Immunotransmitter cGAMP. *Cell Chem. Biol.* **27**, 1347-1358.e5 (2020).

81. Sharma, S. *et al.* Abstract 1932: Discovery of ENPP1 inhibitors as agonists of STING pathway. *Cancer Res.* **78**, 1932–1932 (2018).

82. Gonugunta, V. K. *et al.* Trafficking-Mediated STING Degradation Requires Sorting to Acidified Endolysosomes and Can Be Targeted to Enhance Anti-tumor Response. *Cell Rep.* **21**, 3234–3242 (2017).

83. Bakhoum, S. F. *et al.* Chromosomal instability drives metastasis through a cytosolic DNA response. *Nature* **553**, 467 (2018).

84. Sivick, K. E. *et al.* Magnitude of Therapeutic STING Activation Determines CD8+ T Cell-Mediated Anti-tumor Immunity. *Cell Rep.* **25**, 3074-3085.e5 (2018).

85. Flood, B. A., Higgs, E. F., Li, S., Luke, J. J. & Gajewski, T. F. STING pathway agonism as a cancer therapeutic. *Immunol. Rev.* **290**, 24–38 (2019).

86. Abe, T. *et al.* STING Recognition of Cytoplasmic DNA Instigates Cellular Defense. *Mol. Cell* **50**, 5–15 (2013).

87. Stetson, D. B. & Medzhitov, R. Recognition of Cytosolic DNA Activates an IRF3-Dependent Innate Immune Response. *Immunity* **24**, 93–103 (2006).

88. Abe, T. & Barber, G. N. Cytosolic-DNA-Mediated, STING-Dependent Proinflammatory Gene Induction Necessitates Canonical NF-κB Activation through TBK1. *J. Virol.* **88**, 5328–5341 (2014).

89. Apostolou, E. & Thanos, D. Virus Infection Induces NF-κB-Dependent Interchromosomal Associations Mediating Monoallelic IFN-β Gene Expression. *Cell* **134**, 85–96 (2008).

90. Hu, J. *et al.* Chromosome-specific and noisy IFNB1 transcription in individual virus-infected human primary dendritic cells. *Nucleic Acids Res.* **35**, 5232–5241 (2007).

91. Modulation of cytokine-induced HIV gene expression by competitive binding of transcription factors to the coactivator p300. *EMBO J.* **17**, 3124–3134 (1998).

92. Lipniacki, T., Paszek, P., Brasier, A. R., Luxon, B. A. & Kimmel, M. Stochastic Regulation in Early Immune Response. *Biophys. J.* **90**, 725–742 (2006).

93. Restifo, N. P. *et al.* Loss of Functional Beta 2 -Microglobulin in Metastatic Melanomas From Five Patients Receiving Immunotherapy. *JNCI J. Natl. Cancer Inst.* **88**, 100–108 (1996).

94. Sade-Feldman, M. *et al.* Resistance to checkpoint blockade therapy through inactivation of antigen presentation. *Nat. Commun.* **8**, 1136 (2017).

95. Zaretsky, J. M. *et al.* Mutations Associated with Acquired Resistance to PD-1 Blockade in Melanoma. *N. Engl. J. Med.* **375**, 819–829 (2016).

96. Koopman, L. A., Corver, W. E., van der Slik, A. R., Giphart, M. J. & Fleuren, G. J. Multiple Genetic Alterations Cause Frequent and Heterogeneous Human Histocompatibility Leukocyte Antigen Class I Loss in Cervical Cancer. *J. Exp. Med.* **191**, 961–976 (2000).

97. McGranahan, N. *et al.* Allele-Specific HLA Loss and Immune Escape in Lung Cancer Evolution. *Cell* **171**, 1259-1271.e11 (2017).

98. Shukla, S. A. *et al.* Comprehensive analysis of cancer-associated somatic mutations in class I HLA genes. *Nat. Biotechnol.* **33**, 1152–1158 (2015).

99. Trujillo, J. A. *et al.* Secondary resistance to immunotherapy associated with β-catenin pathway activation or PTEN loss in metastatic melanoma. *J. Immunother. Cancer* **7**, 295 (2019).

100. Salmon, H. *et al.* Expansion and Activation of CD103 + Dendritic Cell Progenitors at the Tumor Site Enhances Tumor Responses to Therapeutic PD-L1 and BRAF Inhibition. *Immunity* **44**, 924–938 (2016).

101. Gaillard, H., García-Muse, T. & Aguilera, A. Replication stress and cancer. *Nat. Rev. Cancer* **15**, 276–289 (2015).

102. Martin, S. K., Tomida, J. & Wood, R. D. Disruption of DNA polymerase ζ engages an innate immune response. *Cell Rep.* **34**, 108775 (2021).

103. Reisländer, T. *et al.* BRCA2 abrogation triggers innate immune responses potentiated by treatment with PARP inhibitors. *Nat. Commun.* **10**, 3143 (2019).

104. Erdal, E., Haider, S., Rehwinkel, J., Harris, A. L. & McHugh, P. J. A prosurvival DNA damage-induced cytoplasmic interferon response is mediated by end resection factors and is limited by Trex1. *Genes Dev.* **31**, 353–369 (2017).

105. Fuertes, M. B., Woo, S.-R., Burnett, B., Fu, Y.-X. & Gajewski, T. F. Type I interferon response and innate immune sensing of cancer. *Trends Immunol.* **34**, 67–73 (2013).

106. Sarasin, A. & Kauffmann, A. Overexpression of DNA repair genes is associated with metastasis: A new hypothesis. *Mutat. Res. Mutat. Res.* **659**, 49–55 (2008).

107. Abida, W. *et al.* Analysis of the Prevalence of Microsatellite Instability in Prostate Cancer and Response to Immune Checkpoint Blockade. *JAMA Oncol.* **5**, 471–478 (2019).

108. Wang, Z. *et al.* Comutations in DNA Damage Response Pathways Serve as Potential Biomarkers for Immune Checkpoint Blockade. *Cancer Res.* **78**, 6486–6496 (2018).

109. Sharma, S. *et al.* Role of MGMT in Tumor Development, Progression, Diagnosis, Treatment and Prognosis. *ANTICANCER Res.* 10 (2009).

110. Mazzu, Y. Z. *et al.* A Novel Mechanism Driving Poor-Prognosis Prostate Cancer: Overexpression of the DNA Repair Gene, Ribonucleotide Reductase Small Subunit M2 (RRM2). *Clin. Cancer Res.* **25**, 4480–4492 (2019).

111. Wu, Z., Wang, Y.-M., Dai, Y. & Chen, L.-A. POLE2 Serves as a Prognostic Biomarker and Is Associated with Immune Infiltration in Squamous Cell Lung Cancer. *Med. Sci. Monit. Int. Med. J. Exp. Clin. Res.* **26**, e921430 (2020).

112. Guo, E. *et al.* The Clinical Significance of DNA Damage Repair Signatures in Clear Cell Renal Cell Carcinoma. *Front. Genet.* **11**, 593039 (2020).

113. Mathews, L. A. *et al.* Increased Expression of DNA Repair Genes in Invasive Human Pancreatic Cancer Cells. *Pancreas* **40**, 730–739 (2011).

114. Kauffmann, A. *et al.* High expression of DNA repair pathways is associated with metastasis in melanoma patients. *Oncogene* **27**, 565–573 (2008).